

## 23. SEDIMENTARY PETROLOGY AND STRUCTURES OF MESSINIAN EVAPORITIC SEDIMENTS IN THE MEDITERRANEAN SEA, LEG 42A, DEEP SEA DRILLING PROJECT

Robert E. Garrison,<sup>1</sup> B. Charlotte Schreiber,<sup>2</sup> Daniel Bernoulli,<sup>3</sup> Frank H. Fabricius,<sup>4</sup> Robert B. Kidd,<sup>5</sup> and Frederic Mélières<sup>6</sup>

### ABSTRACT

Analysis of the petrology and sedimentary structures of Messinian evaporites recovered during Leg 42A yields tentative interpretations of the depositional environments at the various sites. At Site 371, on the southern edge of the Balearic Abyssal Plain, coring retrieved about 2 meters of nodular to laminated anhydrite overlying 2 meters of barren dolomitic mudstone. We interpret this sequence as part of a prograding sabkha cycle. Site 372, on the flank of the East Menorca Rise, contained a thin Messinian sequence of laminated and nodular gypsum with minor dolomitic marls; these rocks lie stratigraphically between pelagic nannofossil marls. The most prominent lithology at Site 372 is laminated gypsum which contains cross bedding, ripple marks, and other indications of current deposition. We believe deposition of this gypsum occurred in a very shallow water evaporite flat that may have been exposed subaerially from time to time.

Evaporitic sediments at Site 374, in the Ionian Sea, comprise a sequence beginning with halite and nodular anhydrite, and progressing stratigraphically upward into cycles of gypsum and dolomitic mudstone and then into dolomitic marl. This succession records a progressive decrease in average salinity as well as an increase in average water depth. The gypsum-mudstone cycles were the result of shorter term fluctuations of water level that produced depositional environments ranging from shallow subaqueous to subaerial.

Coring at Sites 375 and 376, west of Cyprus in the eastern Mediterranean, yielded a variety of Messinian evaporitic rocks including halite, anhydrite, and several kinds of gypsum. Most prominent among the latter are laminated gypsum, selenite, and resedimented gypsiferous deposits (gypsarenite and gypsrudite). Deposition of all of these evaporitic rocks occurred in either very shallow subaqueous or subaerial environments. Lying stratigraphically above them is a sequence of Messinian dolomitic marlstones with interbedded turbiditic arenite and siltites, indicating markedly less saline conditions and deeper water.

Coarse selenitic gypsum was the main deposit of Messinian age recovered at Site 378, in the North Cretan Basin. Precipitation of this gypsum occurred in shallow water. Periodic influxes of less saline water caused some dissolution of the selenite and produced dissolution breccias of slightly reworked selenite crystals. At least brief periods of subaerial exposure are indicated by the presence of small amounts of dolomitic caliche breccia.

<sup>1</sup> Earth Sciences Board, University of California, Santa Cruz, California,

<sup>2</sup> Department of Earth and Environmental Sciences, Queens College, City University of New York, Flushing, New York, U.S.A.

<sup>3</sup> Geologisch-Palontologisches Institut der Universität, Basel, Switzerland.

<sup>4</sup> Institut für Geologie, Technische Universität, München, Germany.

<sup>5</sup> Institute of Oceanographic Sciences, Wormley, Godalming, Surrey, United Kingdom.

<sup>6</sup> Laboratoire de Géologie Dynamique, Université de Paris, France.

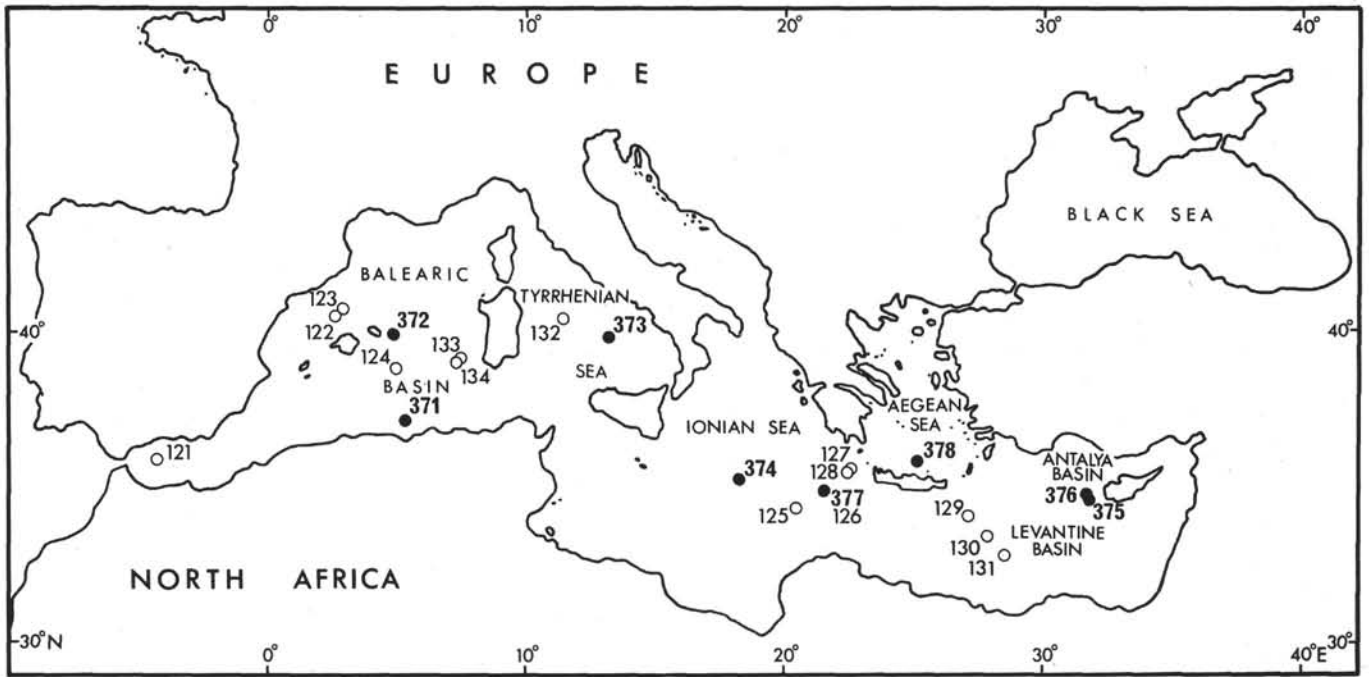


Figure 1a. Locations of DSDP drilling sites in the Mediterranean (Legs 42A and 13).

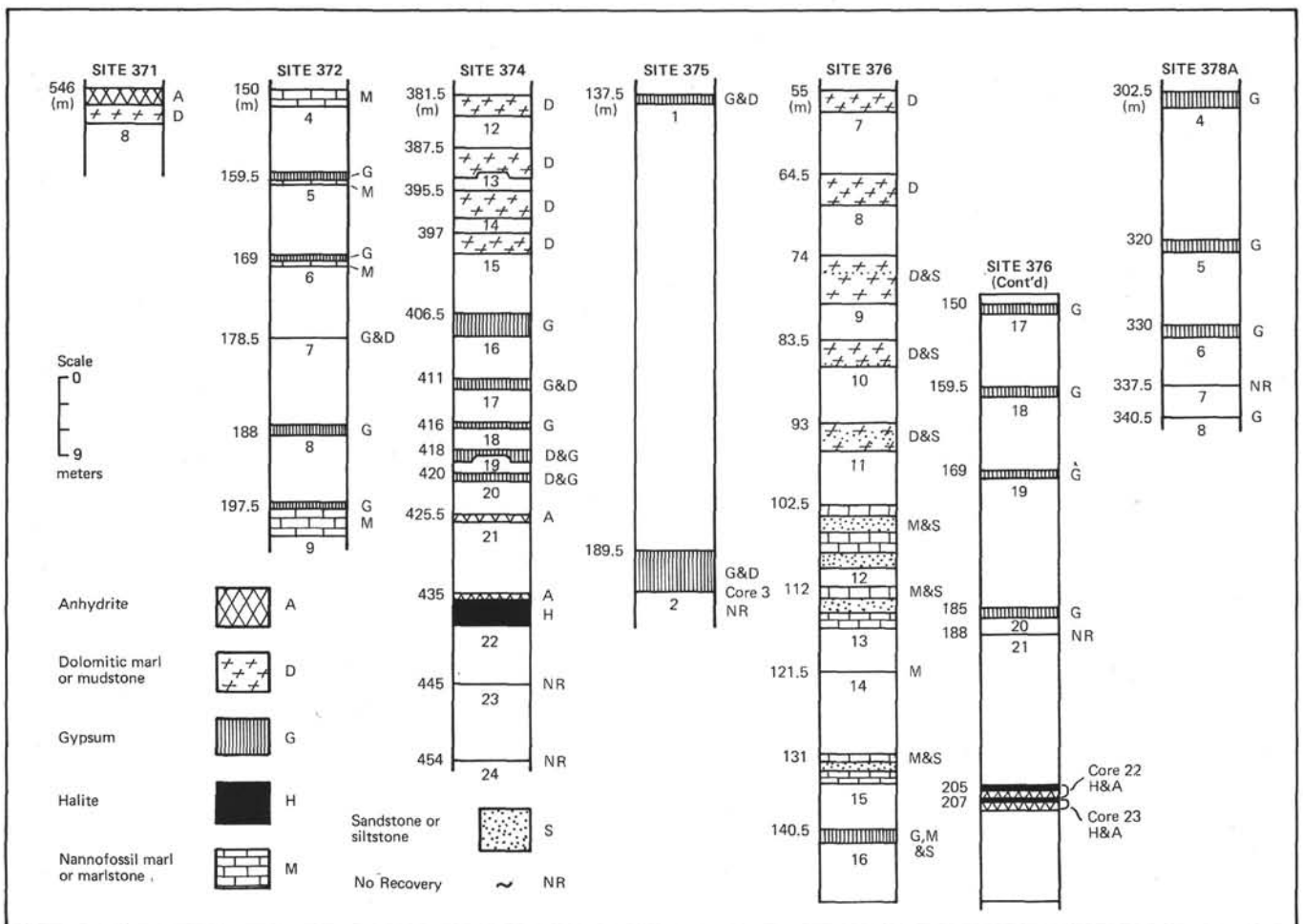


Figure 1b. Schematic presentation of Messinian sediments recovered during Leg 42A. Subbottom depths in meters to left of columns. Core numbers are below the lithologic symbols.

## INTRODUCTION

During Leg 42A we recovered evaporitic sediments of late Miocene age at Sites 371, 372, 374, 375, 376, and 378 (Figures 1a and 1b). Each of these sites had different sequences of evaporites. The Messinian at Site 371 is dominated by nodular anhydrite, while that at Sites 372 and 378 is mainly laminated gypsum and selenitic gypsum, respectively. Site 374 contains a halite to marlstone sequence within which are several mudstone-gypsum cycles. Sites 375 and 376, located adjacent to one another, have a somewhat similar sequence beginning with halite, but the upper part of the succession is dominated by deposits of clastic gypsum. Considerable variability thus exists between these sites, and this no doubt reflects the complexity of paleogeography and events in the Mediterranean region during Messinian time.

The individual site chapters (this volume) hold systematic descriptions and some interpretations of Messinian evaporitic rocks. In the following pages, we have attempted to expand this information with particular attention to petrography, sedimentary structures, and the vertical succession of facies, especially the repetition of facies in cycles, with the final aim of environmental reconstruction.

We wish to emphasize three limitations to the data with which we have worked. One limitation is imposed by the fragmentary core recovery at most sites, mainly a result of mechanical problems. The second results because we sampled only the upper few meters of evaporitic sections which are a kilometer or more in thickness at nearly every site. The size of our samples imposes a third limitation. Among other things, small diameter cores do not allow assessment of the lateral continuity (or lack of same) of sedimentary structures, an aspect of particular importance in the interpretation of evaporitic rocks (Dean et al., 1975; Wardlaw and Christie, 1975; Vonder Haar, 1976). Thus many of our interpretations rely heavily upon comparisons with similar, more completely exposed sequences, both ancient and modern, in other regions. In particular, we have made frequent comparisons of late Miocene evaporites from Leg 42A with contemporaneous rocks in the Gesesso-Solfifera Formation of Sicily (Ogniben, 1957; Selli, 1973; Decima and Wezel, 1971, 1973; Richter-Bernburg, 1973; Nesteroff, 1973b; Schreiber, 1974; Schreiber and Friedman, 1976; Schreiber et al., 1976).

 SITE 371, SOUTHERN EDGE OF THE  
BALEARIC ABYSSAL PLAIN

Messinian sediments recovered at Site 371 consist of about 2 meters of dolomitic mudstone overlain by 2 meters of anhydrite, all in Core 8 (Figure 2). An estimated 6 meters of sand, possibly equivalent to the Arenazzolo at the top of the Gesesso-Solfifera Formation in Sicily, apparently occurs above the anhydrite and is part of an uncored interval between Cores 7 and 8 (see discussion in Site 371 Report, this volume). The dolomitic mudstone (subdivision 10 on Figure 2) is

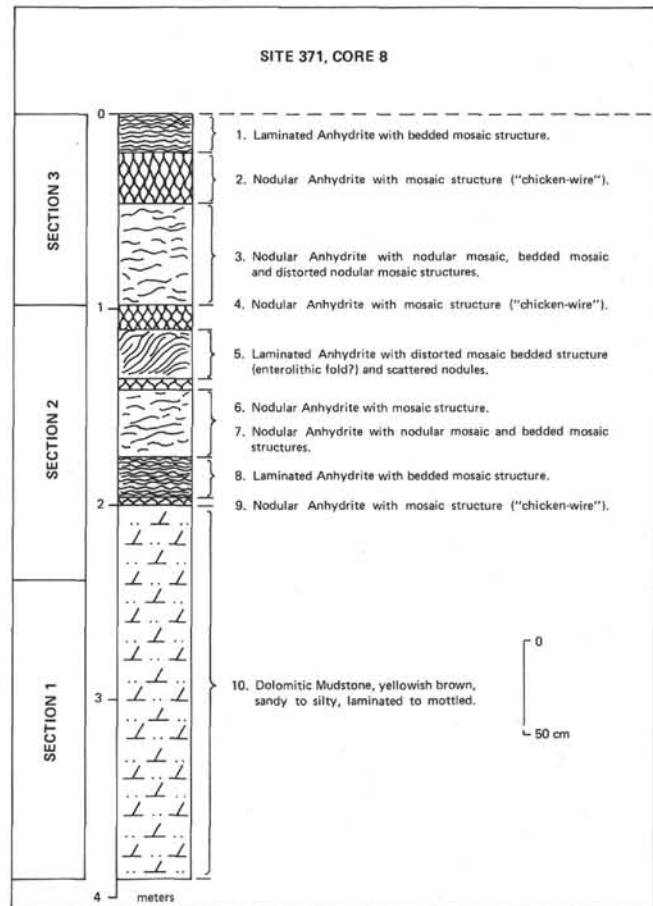


Figure 2. Messinian evaporitic sediments recovered at Site 371. Terminology of anhydritic rocks is after Maiklem et al. (1969). Units 1-10 are informal lithologic divisions (see text).

yellowish brown and sandy to silty, has laminated to mottled structure, and lacks organic burrows. Locally, it contains small displacive nodules of anhydrite, partly altered to gypsum (e.g., Core 8, Section 3, 65-66 cm). As noted in the Site 371 report, both calcite and dolomite are present in about equal amounts, the dominant clay minerals are illite, chlorite, and kaolinite, and quartz grains have frosted surfaces. In places, the dolomitic mudstone becomes quite sandy (Figure 6A), with up to 25% detrital quartz, feldspar, gypsum, chlorite, lithic fragments (including chert and limestone), and plant fragments.

For convenience of discussion, we divide the anhydritic rocks into nine informal lithologic subdivisions based on the dominant structure present (Figure 2). The terminology employed is modified from that proposed for anhydritic structures and textures by Maiklem et al. (1969). The nine subdivisions of anhydritic rocks consist of repetitions of the three kinds of intervals described below.

**Laminated Anhydrite With Bedded Mosaic Structure (Figure 3)**

This forms lithologic subdivisions 1, 5, and 8 (Figure 2), each 20 to 25 cm thick. The main structure is



Figure 3. *Laminated anhydrite, Site 371, core photograph (371-8-1, 54-61 cm).*

laminae, 0.5 to 2.0 cm thick, of milky white anhydrite separated by thin ( $<0.25$  mm), dark gray to dark gray-brown, wavy to discontinuous seams of organic-rich dolomite. The character of the bedding varies from even and nearly flat (especially in subdivision 8) to wavy with small amplitude folds ( $<1$  cm) to discontinuous. Within the anhydrite laminae the predominant structure is coalesced, very small anhydrite nodules averaging about 1 mm in diameter. These nodules are tightly packed to form relatively pure calcium sulfate layers, but in some cases small amounts of impurities (chiefly light brown, fine-grained dolomite) are squeezed between the nodules.

Microscopically the anhydrite laminae consist of densely packed, elongate anhydrite laths (Figure 6[B]) with maximum dimensions mostly less than  $75 \mu\text{m}$ . Some crystals range up to  $500 \mu\text{m}$  long. Overall, most of the anhydrite crystals show random orientation, a texture termed decussate (Shearman and Fuller, 1969) or subfelted to felted (Maiklem et al., 1969). Some parts of the rock have an aligned-felted texture in which anhydrite laths showed preferred orientation

parallel or subparallel to bedding, a texture identical to that found in anhydrite nodules formed beneath modern Persian Gulf sabkhas (Figure 6[D]; Shearman, 1971). Locally there are also stellate clusters of coarse anhydrite crystals, and the tops of some anhydrite laminae consist of thin ( $<0.25$  mm) zones of grayish, translucent anhydrite above the normal milky white variety. Within these zones, which contain less fine-grained impurities than adjacent anhydrite crystals, elongate anhydrite crystals have a preferred orientation perpendicular to bedding, suggesting that crystals grow in that direction.

Scattered through the anhydrite crystals are a few euhedral carbonate rhombs (probably dolomite) and patches where anhydrite is apparently replaced by somewhat coarser, secondary gypsum.

Laminated anhydrite in lithologic subdivision 5 is highly disturbed, with layers inclined up to  $50^\circ$  from the horizontal (Figure 2). This interval resembles some of the larger enterolithic folds, found, for example, in layered anhydrite below Persian Gulf sabkhas (Butler, 1970).

#### **Nodular Anhydrite With Nodular Mosaic to Bedded Mosaic Structure (Figure 4)**

These lithographic subdivisions (numbers 3 and 7, Figure 2) are the thickest of the three kinds of anhydrite, ranging up to 50 cm thick. Most distinctive is their variety of structures which include nodular mosaic, bedded mosaic, distorted nodular mosaic, distorted bedded mosaic, and mosaic structures (cf. Maiklem et al., 1969). The most common type is nodular mosaic structure, consisting of small anhydrite nodules, 2 to 4 cm across, which are separated from one another by gray dolomitic matrix rich in organic matter. The boundaries of many nodules are somewhat indistinct, and the nodules seem to merge into the surrounding dark matrix (Figure 4).

The predominant nodular mosaic structure of subdivisions 3 and 7 appears to grade into all of the other kind of anhydrite structures, particularly, however, into bedded mosaic structure. There are also transitions from rather loosely packed anhydrite nodules surrounded by abundant organic matter—and dolomite-rich matrix to tightly packed nodules with mosaic or “chicken-wire” structure. Some intervals show distorted nodular mosaic structure with nodular bodies flattened parallel to bedding, others have small enterolithic folds.

On a microscopic scale the nodular anhydrite in these intervals consists of tightly packed anhydrite crystals, mostly less than  $50 \mu\text{m}$  long, with felted to aligned felted textures. Superimposed on this dominant texture are stellate clusters of anhydrite laths up to  $500 \mu\text{m}$  long (Figure 6[C]), and scattered, irregular laths of gypsum that replaces anhydrite. Inclusions and small wisps of fine-grained dolomite, dark brown organic matter, and rare pyrite are dispersed through the felted matrix, but tend to be excluded from the stellate crystal aggregations, suggesting the latter may represent a diagenetic overprint.

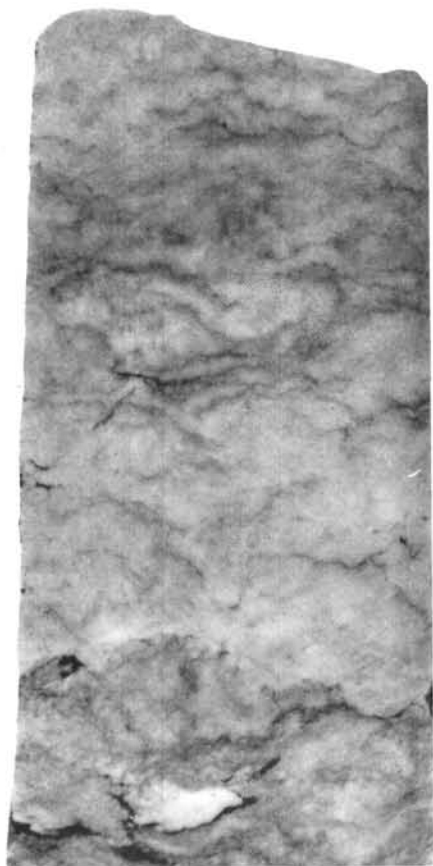


Figure 4. *Anhydrite with nodular mosaic structure, Site 371, core photograph. Scale bar is 1 cm (371-8-1, lower half).*

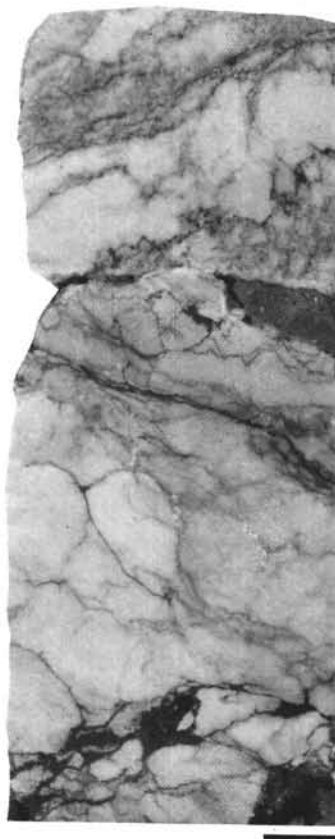


Figure 5. *Anhydrite with mosaic structure ("chicken-wire structure"), Site 371, core photograph. Scale bar is 1 cm (371-8-1, 65-74 cm).*

#### **Nodular Anhydrite With Mosaic Structure ("chicken-wire structure") (Figure 5)**

Anhydrite of this kind constitutes lithologic subdivisions 2, 4, 6, and 9, which are generally the thinnest of the subdivisions, ranging from a few centimeters to about 25 cm thick (Figure 2). The chief characteristic is tightly packed, milky white anhydrite masses or nodules which are approximately equidimensional and between which appreciable matrix is lacking. The internodular areas are very thin seams of black material rich in organic material or brownish dolomitic sediment. This is the type of rock commonly called "chicken-wire anhydrite" by petroleum geologists. The anhydrite masses generally have sharp boundaries, are of moderate size (2 to 5 cm across), and largely lack preferred orientation. Within lithologic subdivision 2 are two thin and discontinuous layers of soft brown dolomitic mud. We are uncertain whether these are in situ or are injected drilling artifacts, but we suspect the latter.

#### **Interpretation**

Studies of tidal flats in the Persian Gulf region during the past 15 years have affirmed the association

of nodular anhydrite with sabkha sedimentation (Kinsman, 1969). Dean et al. (1975) and Wardlaw and Christie (1975), among others, have noted, however, that anhydrite nodules are diagenetic alteration products which may replace calcium sulfate sediments of diverse origins, including those formed in deep water. Nevertheless, we find a remarkable similarity between the dolomitic mudstone-anhydrite sequence at Site 371 and the Holocene sabkha cycle of the Trucial Coast area adjoining the Persian Gulf (Butler, 1970) as well as sabkha cycles identified in the geologic record (e.g., Bosellini and Haride, 1973; Friedman, 1973; Bebout and Maiklem, 1973; Stoffers and Kuehn, 1974). Employing this analog, we interpret the transition at Site 371 from dolomitic mudstone below to anhydrite above as: (1) a shoaling upward or regressive sequence, and (2) a change from a regime of probable subaqueous deposition for the dolomitic mudstone of subdivision 10 (Figure 2) to an environment dominated by subaerial diagenetic processes. The most important of these processes was the displacive growth of early diagenetic anhydrite masses, either by direct precipitation in highly concentrated pore waters or by replacement of gypsum (Kinsman, 1969; Butler, 1970). The probable depositional environments thus ranged from shallow subaqueous to sabkha.

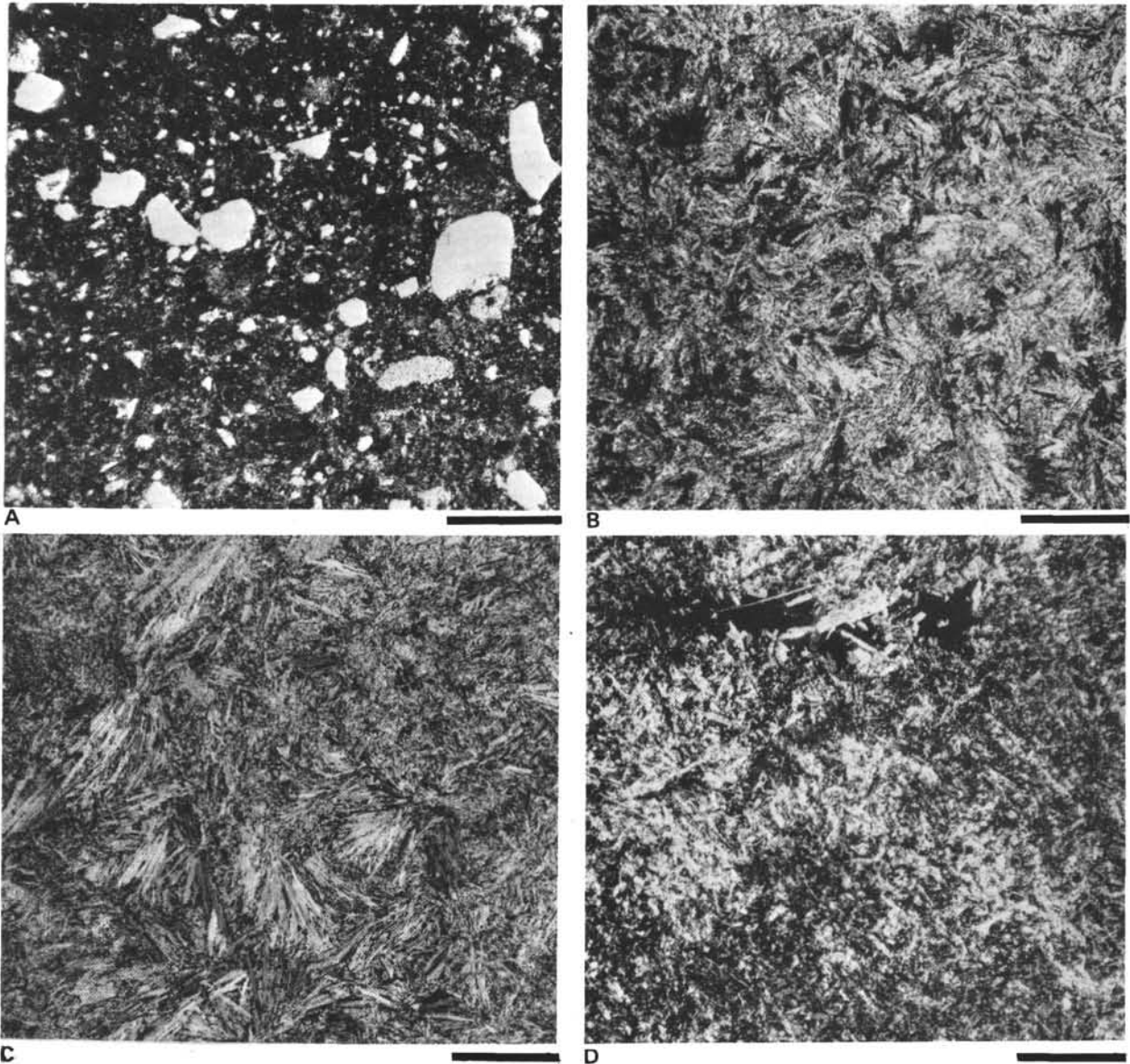


Figure 6. Photomicrographs of evaporitic rocks at Site 371. Scale bars are 500  $\mu\text{m}$ . A, plain light, B, C, and D, crossed nicols. (A) Dolomitic mudstone with detrital clasts of quartz, feldspar, and other components in matrix of fine-grained dolomite (371-8-3, 65-66 cm). (B) Felted anhydrite laths from laminated anhydrite (371-8-2, 73-76 cm). (C) Stellate anhydrite laths, in nodular mosaic anhydrite (371-8-1, 141-146 cm). (D) Felted anhydrite laths from Holocene anhydrite nodule, Trucial Coast sabkha, Persian Gulf. Dark areas at top are irregularly shaped vugs.

The variations of structures within the upper 2 meters of anhydrite (Figure 2) were noted previously. We interpret these structures as follows:

1) The laminated anhydrite (subdivisions 1, 5, and 8) closely resembles certain modern and ancient laminated algal sediments (stromatolites) which have been modified by diagenetic displacive growth of calcium sulfate minerals within the sediment (cf. Butler, 1970; Shearman and Fuller, 1969; Horodyski and Vonder Haar, 1975; Vonder Haar, 1976).

2) Anhydrite with "chicken-wire" structure (subdivisions 2, 4, 6, and 9) appears to represent a more advanced stage of diagenetic modification, where continued growth of anhydrite nodules and minimal com-

paction allowed squeezing of pre-existing sediment and organic matter into wisps and thin seams.

3) Anhydrite with nodular mosaic and a variety of other structures (subdivisions 3 and 7) appears to represent the most advanced stage of diagenesis and displacive crystal growth. Discontinuous internodular seams and matrix represent preexisting sediment, possibly including algal mats, although we observed no algal filaments.

Shearman and Fuller (1969) suggested that variations of these kinds might be produced by differences in compressibility and drainage of the host sediment in which anhydrite grew. Butler (1970, fig. 14, p. 134) has demonstrated how anhydrite structures may be

related to distance from the subaqueous regime and to burial depth in prograding sediments of modern sabkhas. Laminated anhydrite like type 1 at Site 371 is formed in mid-sabkha regions when gypsum crystals within algal laminations are replaced by anhydrite. Nodular anhydrites like types 2 and 3 above develop also in mid-sabkha regions, but become particularly prominent in the more landward portions of the sabkha, in diagenetic regimes dominated by mixtures of continental groundwater with concentrated marine pore waters.

We may thus postulate that the laminated anhydrites formed under more nearly subaqueous conditions, and that the anhydrites with nodular mosaic and mosaic ("chicken-wire") structures represent more subaerial settings dominated by diagenesis. In this interpretation, the alternations of types of anhydrite (Figure 2) may be viewed as responses to very slight fluctuations in water level (cf. Bebout and Maiklem, 1973).

Somewhat similar Messinian cycles of nodular anhydrite and barren dolomite muds were recovered during Leg 13 at Site 124 on the Balearic Rise (Ryan, Hsü, et al., 1973; Nesteroff, 1973a; Friedman, 1973) and during Leg 23 at Site 225 in the Red Sea (Stoffers and Kuehn, 1974).

#### SITE 372, EAST MENORCA RISE

The Messinian sediments recovered at Site 372 consist of dolomitic marls and laminated gypsum retrieved in Cores 4 through 9, over a 54-meter interval between subbottom depths of 150 and 204 meters. Recovery within this interval, however, was sporadic and relatively sparse. The most complete recovery of evaporites was in Core 8, and most of the discussion below deals with the laminated gypsum of this core.

#### Laminated Gypsum of Core 8

##### Structures

The most prominent set of laminations vary in thickness from about 0.3 to 1.0 cm thick (Figures 7 to 11). Each lamination of this kind is composed of two *sublaminae* (Figures 8 and 9).

1) A fine-grained basal sublamina, commonly itself very finely subdivided into extremely thin layers here called *micro-laminae*. These basal sublaminae are composed of micritic carbonate, finely dispersed gypsum crystals, and possibly some argillaceous material. For purposes of discussion, this is here designated as the *F Sublamina*.

2) A coarser upper sublamina, here called the *C Sublamina*, which is relatively carbonate-free and is composed of a reversely graded mosaic of interlocking gypsum crystals. The tops of the C sublaminae are relatively sharp beneath the overlying F sublamina, whereas the contacts between F and overlying C sublaminae are transitional. The sharp upper surfaces of the C Sublaminae vary in geometry from even and very flat, to irregular and serrated to wavy. Very commonly the relief of the irregular upper "C" sur-



Figure 7. Laminated gypsum, Site 372, core photograph. Note irregular shaped gypsum crusts (dark gray), including upward growth of coarse gypsum crystals at bottom. Scale bar is 1 cm (372-8-2).

faces became filled in and leveled by deposition of succeeding micro-laminae *within* the F intervals (Figures 7 to 11), i.e., the irregular surface developed before the onset of F sedimentation. Larger scale wavy bedding, however, tended to be propagated upward through several sets of micro-laminae before leveling occurred.

Several variants of the basic pattern of lamination resulted from penecontemporaneous mechanical current action. The most conspicuous of these is rip-up breccias consisting of elongated clasts of the graded gypsum cemented in a matrix of fine-grained gypsum and micritic carbonate (Figure 12). These form intervals up to 22 cm thick (e.g., 101-123 cm, Section 2 of Core 8). They originated by vigorous current or wave erosion of previously lithified gypsum, possibly during storms. These clasts lack the micritic F Sublaminae, probably because the carbonate, in contrast to the gypsum, was not lithified at the time of erosion. Other products of current action include intervals of cross-laminated gypsum which occur throughout Core 8. These vary from planar cross lamination in sets less than 1 cm thick to low angle cross lamination forming sets a few centimeters thick (Figure 13). In both kinds of cross lamination, subsequent current or wave scour has leveled the tops of the small ripple marks. A third type of current-induced structure includes sets of small, asymmetrical ripple marks with very low amplitudes (Figures 14 and 15). Many of these have oversteepened sides. These ripple marks resemble structures which have been termed adhesion ripples or antiriplets and attributed to the adhesion of wind blown sand to a wet surface (Reineck and Singh, 1975, p. 56-67).

##### Petrography

Microscopic study of the laminated gypsum clearly delineates the nature of the reversely graded layers (Figures 7-10 and 15). The F sublaminae are com-

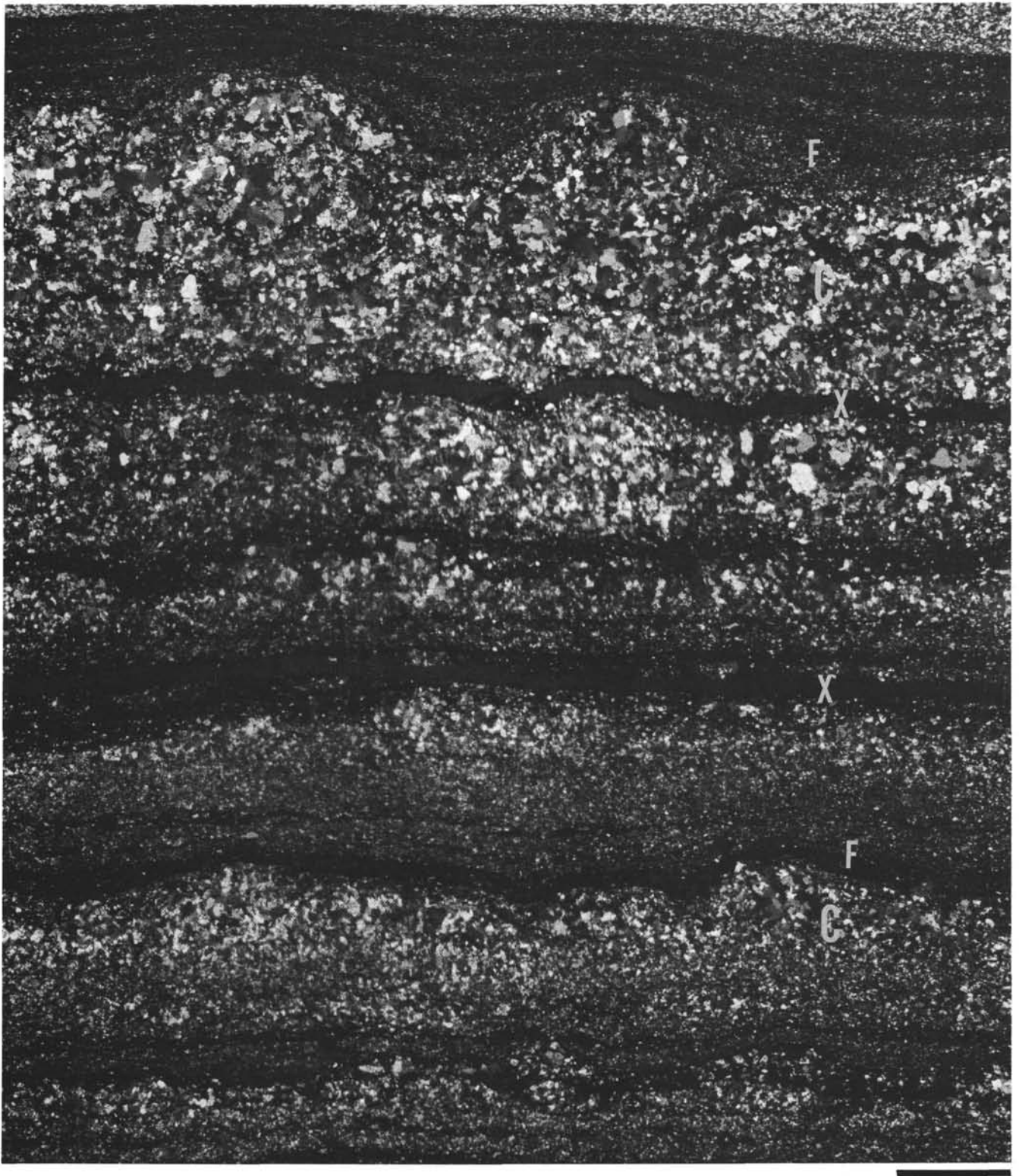


Figure 8. *Laminated gypsum, Site 372, thin-section photograph, crossed nicols. Note reversely graded layers, and draping and infilling of thin, dark micritic micro-laminae above irregular coarse tops of layers. C = coarse-grained, reversely graded sub-laminae, composed mainly of gypsum crystals; F = fine-grained, sub-laminae composed of micro-laminae micrite, fine-grained gypsum particles, and possibly clay minerals; X = cracks (artifacts) in the thin section (372-8-1, 90-95 cm). Scale bar is 2 mm.*

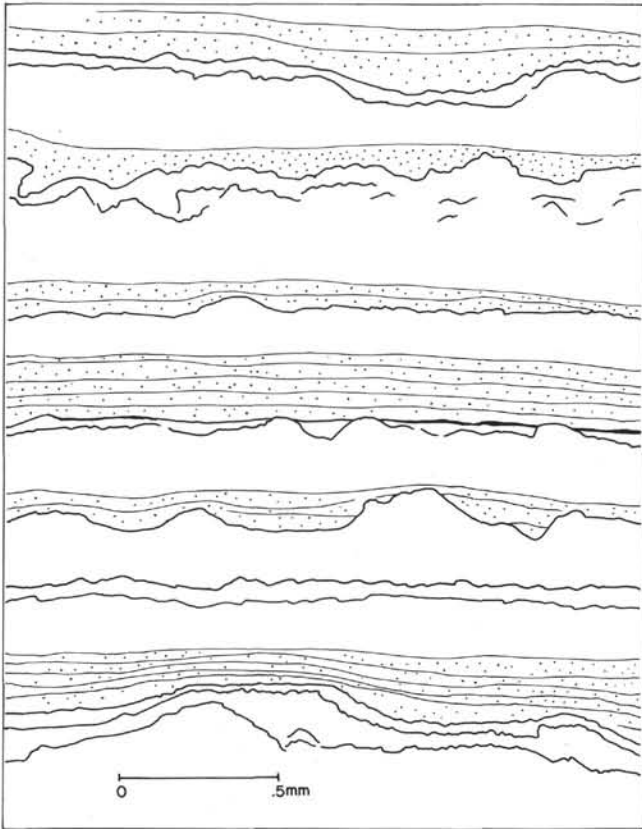


Figure 9. Laminated gypsum, Site 372, drawing of thin section made from a Shadomaster. Clear area = inversely graded gypsum sub-laminae (C), stippled areas with fine lines = sub-laminae containing micro-laminae (F). Heavier wavy lines are organic-rich micro-laminae, possibly the remnants of algal stromatolites disrupted by diagenetic growth of gypsum in the C sub-laminae (372-8-1, 76-79 cm).

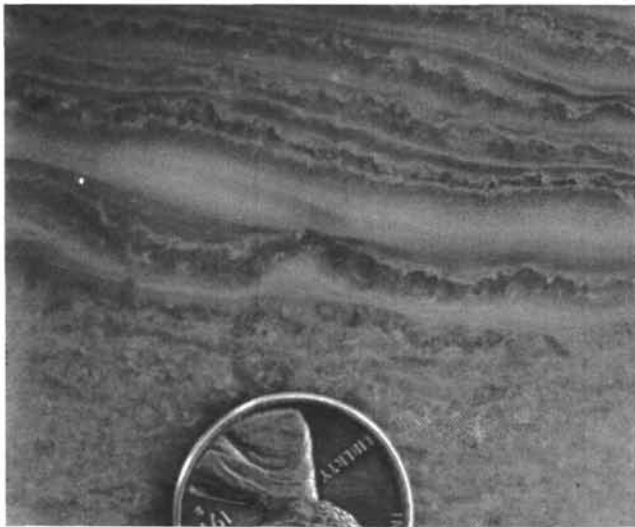


Figure 10. Laminated gypsum, Site 372, core photograph. Note irregular recrystallized upper parts of layers (C sub-laminae, darker areas) and infilling of relief by fine-grained sub-laminae (F). Coin diameter is 1.9 cm (372-8-2).

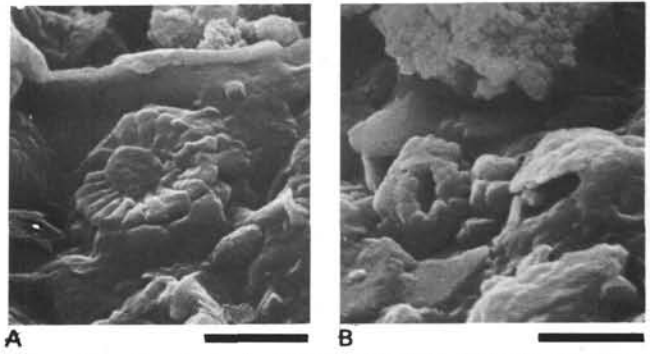


Figure 11. Laminated gypsum, Site 372, scanning electron micrographs of micrite in F sub-laminae. Note coccoliths surrounded by fine-grained calcite and possibly clay minerals. Scale bars are 2  $\mu$ m (372-8-2, 51 cm).



Figure 12. Laminated gypsum, Site 372, core photograph. This is a rip-up breccia composed of elongated clasts of laminated gypsum. Note evenly laminated gypsum at bottom. Coin diameter is 1.9 cm (372-8-2).

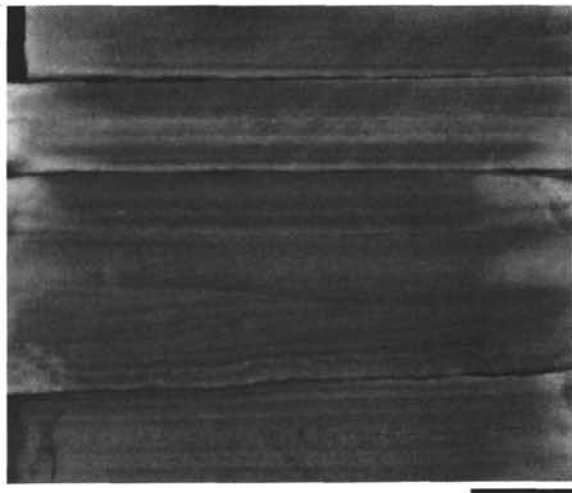


Figure 13. *Laminated gypsum, Site 372, core photograph. Note small scale cross-lamination just below the middle, Scale is 1 cm (372-8-1, 50-55 cm).*

posed of micrite in which are embedded equigranular, anhedral to subhedral gypsum crystals with maximum dimensions in the range of 20 to 70  $\mu\text{m}$ . Some F sublaminar also contain elongated gypsum crystals aligned parallel to bedding. Micritic carbonate and occasional abraded-appearing foraminifers are scattered through the F sublaminar, but micritic carbonate tends to be most abundant in the basal part, just above the C sublaminar. Scanning electron microscopy shows the presence of a few coccoliths in the F sublaminar (Figure 11); coccoliths seem, however, not to be as abundant in these rocks as Rochy (1976) has reported for laminated gypsum from Sicily.

C sublaminar consist of equant, blocky crystals which are anhedral to subhedral and mostly in the size range of 100 to 200  $\mu\text{m}$ , with some crystals being up to 800  $\mu\text{m}$  in maximum dimension. The texture is granoblastic with the gypsum occurring as interlocking crystals that lack preferred orientation. In contrast to most F sublaminar, C sublaminar seem to have undergone extensive diagenetic recrystallization.

C sublaminar also tend to be clearer and to contain less intercrystalline micrite and other impurities, although there are some exceptions. The highest concentrations of the carbonate are in the basal portions of the F sublaminar. The upper surfaces of many C sublaminar are covered by dark, irregular thin micro-laminar that are rich in organic matter and were possibly algal stromatolites<sup>7</sup> draped over irregular surfaces (Figures 8 and 9). Similar organic matter-rich micro-laminar also occur *within* some of the C sublaminar (Figures 8 and 9). The tops of some C sublaminar are capped by thin micro-laminar of clear, rounded gypsum crystals cemented in micritic matrix;

<sup>7</sup>By convention we shall use the term "algal stromatolites," although the original structure may have been a consortium of algal and bacterial colonies and sediment.

these appear to be reworked and abraded grains from the underlying C sublaminar.

As noted, the upper surfaces of C sublaminar vary from flat to wavy. The waviness in some instances takes the form of more or less regular sinusoidal surfaces with typical amplitudes and wavelengths of 2 to 4 mm, in other cases the prominences are more irregularly spaced and have less relief (Figures 8 and 9). Both resemble small ripple marks in cross-section, and it is possible some were originally adhesion ripples or wrinkle marks (Runzelmarken) formed by water movement over a partly cohesive sediment surface (cf. Reineck and Singh, 1975, p. 56). However, petrographic details suggest the origin of the waviness is somewhat more complex. In several instances the C sublaminar upper surfaces are much too irregular and jagged to be a ripple surface (Figure 7). The gypsum crystals beneath the upward protuberances, or "peaks," are typically more coarse-grained and inclusion-free than that in the adjacent valleys; some of the peaks, in fact, appear to be small nodules of secondary gypsum. In a few examples, slightly elongated gypsum crystals extend upward from the peaks as if they had grown upward from a stable, indurated substrate (Figure 7).

Thus a component of the waviness at the top of C sublaminar appears to result from diagenetic recrystallization of gypsum, and conversely dissolution of gypsum may have added further irregularities. The fact that the succeeding F sublaminar acted to fill and level irregularities at the top of underlying C sublaminar (Figures 7-10) is significant in several respects. First, these irregularities must have existed on the sea floor prior to deposition of the overlying micro-laminar (Hardie and Eugster, 1971). This in turn indicates that



Figure 14. *Laminated gypsum, Site 372, core photograph. Note very small, asymmetric ripple marks in lower half. Scale bar is 1 cm (372-8-1, 32-34 cm).*

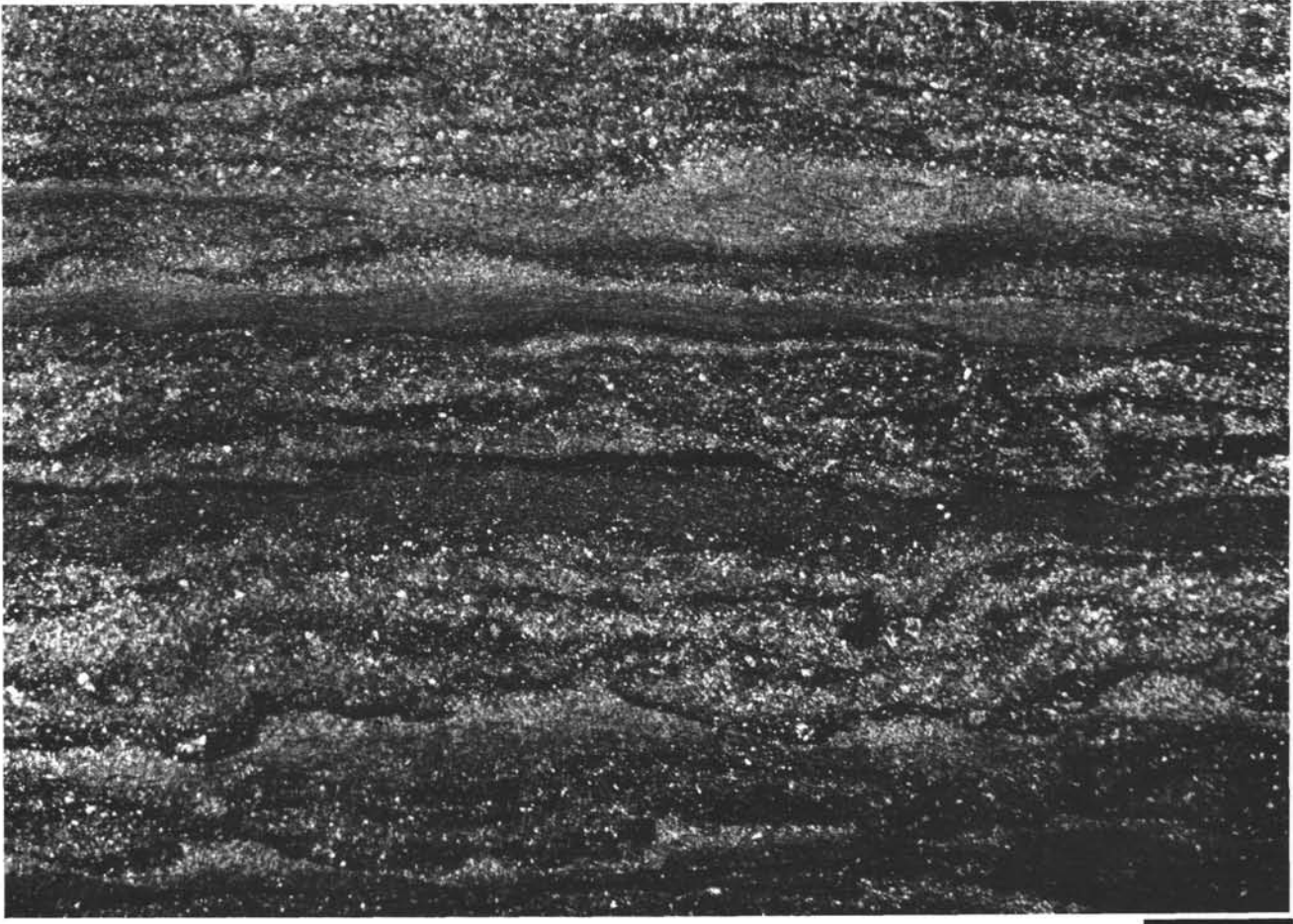


Figure 15. *Laminated gypsum, Site 372, thin-section photograph, partly crossed nicols. Note small irregularities in bedding, many of which appear to be wrinkle marks or adhesion ripples (antiripplets) which have steep upcurrent sides toward the left; note that some of these upcurrent sides are oversteeped, particularly in the lower half. Note also the reversely graded laminae. Scale bar is 2 mm (372-8-1, 32-34 cm).*

the recrystallization and new crystal growth occurred very early in diagenesis (indicated also by the rip-up breccias) and produced a lithified gypsum crust on the sea floor (cf. Schreiber et al., 1976). Various events followed this lithification, in addition to deposition of the normal overlying fine-grained F sublamina. One such event was probably the growth of algal stromatolites on top of some of these crusts or penecontemporaneously with formation of the crusts. Another was occasional current erosion and reworking of the upper part of the lithified crust. This may have created still further irregularity at the top of the crust, or, alternately, acted to reduce the irregularity through erosion. It also produced discontinuous microlaminae of rounded detrital gypsum grains at the base of the next F sublamina.

**Origin of Laminae, Reverse Grading and Depositional Environment in Laminated Gypsum of the Upper Gessoso-Solfifera Formation, Sicily.**

Laminated gypsum similar to that present at Site 372 occurs in the upper Miocene Gessoso-Solfifera Formation of Sicily where a number of workers have

undertaken investigations. The Sicilian laminated gypsum is sometimes called "Balatino," although Schreiber et al. (in press) point out that this term refers to the appearance of beds of broken rock rather than to the laminations. Ogniben (1955, 1957) interpreted the gypsum laminae of the Gessoso-Solfifera Formation as varves, attributing the reversed grading to annual variations in the precipitation of calcium sulfate. Hardie and Eugster (1971) documented a variety of features in laminated gypsum of the Gessoso-Solfifera Formation that indicate current transport and deposition rather than annual precipitation as the dominant depositional process. They postulated that the planar parallel laminae were mechanically deposited storm layers with interlaminae of algal stromatolites and suspension-settled fine carbonate, processes that commonly produced normally graded laminae. They are uncertain about the origin of the reverse graded layering, pointing out that recrystallization had obliterated primary textures; but they felt the inverse grading might be "a variation of the storm layer couplet-type lamination." Their interpretation of the overall depositional environment was nearshore, shallow subaqueous

to subaerial with the gypsum clasts being derived from erosion of selenite crystals that grew on a nearby lagoon floor and/or along an exposed shoreline.

Schreiber et al. (in press), emphasizing the abundance of cross bedding, ripple bedding, and desiccation features, also recognized the importance of mechanical redeposition in genesis of the laminated Sicilian gypsum in very shallow water. They formulated a scheme whereby inversely graded gypsum layers resulted from very early diagenetic recrystallization of primary gypsum. In their view, an influx of less saturated water, a "freshening," caused partial solution of the primary gypsum crystals. Rapid reconcentration of the overlying water in the next cycle, however, yielded recrystallization and lithification in the upper portion of the previously deposited gypsum lamina as well as renewed primary precipitation of the gypsum crystals of the next lamina.

Roche (1976) has reported the discovery of abundant calcareous nanofossils in the micritic laminae between gypsum layers as well as within the gypsum layers themselves. Whereas the calcareous laminae contain what he interprets as a normal marine nanoflora, those found in the gypsum layers comprise a reduced assemblage of dwarf forms. Roche's interpretation thus is that the laminations represent alternating influxes of normal marine water and very saline water (see also discussion of laminations by Heimann in Fabricius et al., this volume).

#### Origin of Laminated Gypsum in Core 8

We interpret the laminated gypsum in Core 8 at Site 372 as being shallow subaqueous sediments, deposited within the zones of photosynthetic activity and periodic strong wave action. This could be, for example, an evaporitic flat or a lagoonal environment. In this interpretation we place strong reliance, along with Hardie and Eugster (1971) and Schreiber et al. (1976), on sedimentary structures and the sequence of structures. The most critical of these are cross bedding, ripple marks, and rip-up breccias, and their repetition in the vertical stratigraphic sequence suggests that the environment was one periodically exposed to high energy events like storms. The presence of possible algal stromatolites tends to support this shallow water interpretation.

Hardie and Eugster (1971) and Schreiber (1974) reported mud cracks in laminated gypsum of the Solfifera Series, a structure which along with others they took as indicative of periodic subaerial exposure. We have found no mud cracks at Site 372. Hardie and Eugster interpreted rip-up breccias identical to those in Core 8 as the result of wave reworking of subaerially hardened crusts. Structures resembling adhesion ripples (Figures 14 and 15) are suggestive of subaerial exposure. According to Reineck and Singh (1975, p. 56) these structures form when dry sand is blown over a smooth moist surface which traps the sand grains. Changes in wind direction produce irregular knobby adhesion warts with oversteepened sides. Conceivably,

some of the relief at the tops of C sublaminae (cf. Figure 8) could have this origin, while other parts of the relief may have originated as ripple marks.

Our observations lead us to agree with Hardie and Eugster (1971) that the laminations resulted from periodic current activity in very shallow water. We believe that the inverse grading of many laminations is a primary depositional feature that was modified by early diagenetic recrystallization. Clifton (1969) has described inversely graded laminae in beach sands; he attributes this structure to upward segregation of coarser and less dense particles within a highly concentrated flowing layer of sand during wave backwash. The presence of abundant micrite and possible algal stromatolites in the laminated gypsum at Site 372 makes a beach origin unlikely there, although it is conceivable that these sediments could occur in the lower shoreface of a low energy beach. However, high density flowing sheets of sand and finer particles, analogous to wave backwash, might also be expected to develop in very shallow water on tidal flats during storms (cf. Reineck and Singh, 1975, p. 359). Storm waves would transport nanoplankton from more open marine environments and mix them with gypsum crystals formed in a more restricted environment. Inverse size grading, developed during deposition from a highly concentrated flow of sediment, would be accentuated during calm periods between storms by neomorphic growth of gypsum on the sediment surface.

Vonder Haar (1976) has described a modern gypsum-bearing evaporate flat that bears some similarity to the environment envisaged above. This is at Laguna Mormona along the Pacific Coast of Baja California. The gypsum deposits there are not a perfect match for those at Site 372, but they have many similarities including inversely graded layers, adhesion ripples, algal mats, and early diagenetic cementation of surface layers of gypsum.

#### Cores 4, 5, 6, and 7

Core 4, the youngest Messinian sediment at Site 372, consists of variegated gray, red, and brown nanofossil marls that locally contain dolomite and pyrite. These marls have fine sandy laminae and some of them contain planktonic and benthic foraminifers which are usually small or dwarf forms.

The limited recovery in Cores 5 and 6 was similar to that of Core 8 and consisted of a few centimeters of laminated gypsum overlying pale red to light gray, laminated marl. The sequence of gypsum structures and textures is similar to that in Core 8 but there are two major differences. Some of the basal portions of the F sublaminae have reddish coloration, possibly reflecting the influx of terrigenously generated hematite. In addition, the interval from about 125 to 135 cm in Section 1, Core 6 is dolomitic mudstone which contains displacive crystals and nodules of gypsum, and discontinuous gypsum layers formed of coalesced nodules and locally showing enterolithic folding. The dolomitic mudstone is strongly laminated and was

possibly of algal stromatolitic origin; however, the mudstones and marls also contain a sparse, dwarfed fauna of planktonic foraminifers. We interpret the gypsum structures as having been formed by secondary precipitation in subaerially exposed carbonate muds in a sabkha setting (cf. Kinsman, 1969; Butler, 1969; Hardie and Eugster, 1971, p. 211; Vonder Haar, 1976). But the presence of dwarf planktonic foraminifers indicates probable periodic influxes of saline water. Retrieval from Core 7 consisted only of two core-catcher samples composed of light brownish gray dolomitic marl and small gypsum nodules.

#### Core 9

Core 9 may be included in this discussion of the evaporitic sediments at Site 372 depending on the full lithologic and biostratigraphic interpretation of this core (see Summary and Conclusions in Site 372 Report, this volume). Two differing biostratigraphic interpretations place a hiatus either at the top of this core, or within the Core at 9-2, 50 cm. We must emphasize that in both interpretations there is agreement that a major part of the Tortonian is missing (representing either about 3.2 m.y. or about 4.7 m.y.); furthermore, evidence from seismic profiling leaves no doubt that such a major hiatus does exist.

In the upper 10 cm of Core 9 are pieces of laminated gypsum like that described in Core 8; these are thought to be downhole contaminants. Below this is about 25 cm of soft bluish gray and white nannofossil ooze that is intensely disturbed by drilling. This is underlain by approximately 105 cm of unburrowed, finely laminated, gray and white marl which contains silt to sand size gypsum crystals. Below this is burrowed nannofossil marl with a normal pelagic marine fauna and flora, and a bathyal assemblage of benthic foraminifers. The laminated marls, in contrast, contain a sparse and restricted flora and fauna or planktonic and benthic foraminifers and nondiversified nannofossils, described in the Site 372 report, this volume and in Cita et al., this volume. Although in scale the laminae of the marls bear a superficial resemblance to those in the overlying gypsum, they contain no evidence of current reworking such as cross lamination. We interpret them as products of subaqueous deposition in an environment increasingly hostile to organisms, probably as the result of increasing salinity. Possibly this was a hypersaline lagoon or a shallow stagnant basin. (See also discussion in Hsü et al., this volume.) In their megascopic characters, these laminated marls bear a remarkable resemblance to coccolith-bearing laminated marls in the Black Sea (Ross and Degens, 1974; Müller and Stoffers, 1974).

#### Possible Cycles

Cores 8 and 9 record a change from laminated marls to laminated gypsum above. Cores 5 and 6 appear to show a similar transition, although in a much less complete fashion because of very limited core recovery. In these cores we thus seem to have glimpses of cycles seen more fully elsewhere (e.g., at Mediterra-

nean Sites 124 and 374 and in the Gessoso-Solfifera Formation of Sicily; see discussions in Heiman and Mascle, 1974; Schreiber et al., 1976), and recording a change from subaqueous marl deposition to more hypersaline conditions of gypsum deposition to (in Core 6) subaerial exposure and displacive precipitation of calcium sulfate in a sabkha setting.

#### SITE 374, IONIAN SEA

Sediments of Messinian age were cored continuously between subbottom depths of 381 and 457 meters, but recovery was only partial within this interval and the two deepest cores (23 and 24) had no recovery. Cores 12 through 15 recovered dolomitic mud and mudstone. Cyclically bedded mudstone and laminated gypsum were recovered in Cores 16 through 20, and Cores 21 and 22 recovered layered anhydrite and halite. A comparison between evaporite land sections on the Ionian Islands to the northeast of Site 374 can be found in Chapter 46 (Fabricius et al., this volume).

#### Dolomitic Mud and Mudstone, Cores 12-15

These are largely barren and unburrowed sediments which are dark greenish gray. X-ray analyses indicate they contain 12%-27% dolomite, 12%-18% quartz, trace to 5% feldspar, and up to 65% clay minerals, mostly illite, smectite, and mixed-layer clays. Numerous small white spheres consist of the magnesium phosphate mineral lüneburgite (Müller and Fabricius, this volume).

These sediments contain no calcareous fossils, and no calcite was detected by X-ray diffraction. Light isotope composition of this sediment (see chapters on isotope geochemistry in this volume) suggests the water was for the most part not marine, but rare occurrences of sponge spicules and radiolarian tests (e.g., in the core-catcher sample of Core 15) indicate occasional marine incursions. Lack of benthic fauna suggests the bottom conditions were stagnant, and the overall environment may have been somewhat like the present Black Sea (Ross and Degens, 1974; Müller and Stoffers, 1974). Origin of the dolomite is uncertain; it may be analogous to the Pliocene-Quaternary dolomite of the Black Sea (Ross, Neprochnov, et al., in press) or dolomite formed subaqueously in west Texas lakes (Parry et al., 1970) through primary precipitation or subaqueous diagenesis.

#### Gypsum-Mudstone Cycles of Cores 16-20

These five cores penetrated an apparently cyclically bedded sequence of mudstones and gypsum between subbottom depths of 406.5 and 425.5 meters. Recovery within the interval, however, was only partial and sporadic, but complete enough to allow reconstruction of a three member cycle. The data used to reconstruct the cycle are shown in Figure 16, an idealized cycle is portrayed in Figure 17, and the descriptions and interpretations below refer to the three members designated as A, B, and C.

**A Member:** The major lithography is olive-gray to black, organic matter-rich, soft dolomitic mudstone.

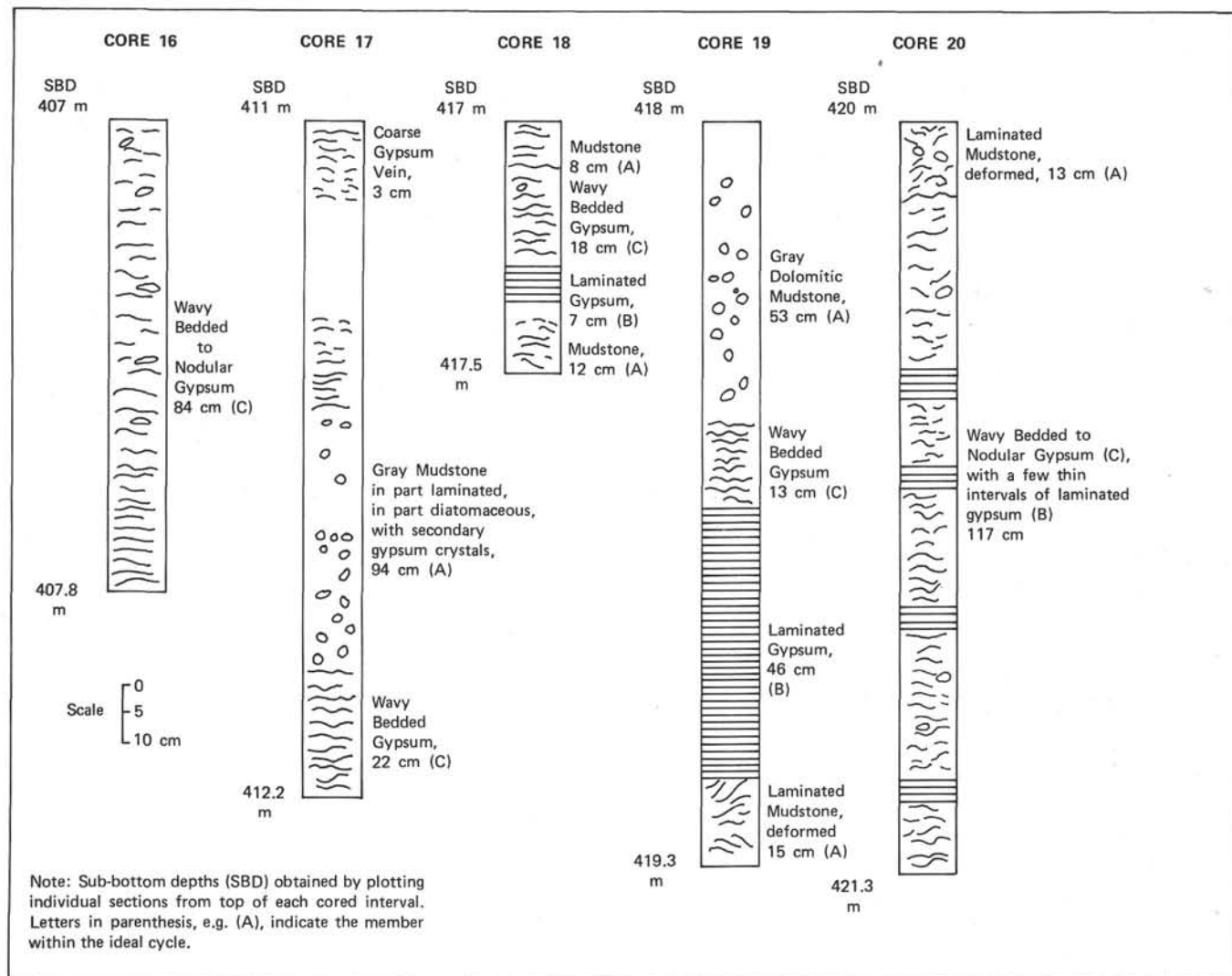


Figure 16. Gypsum-mudstone cycles recovered at Site 374. SBD refers to subbottom depths.

This varies from homogeneous and massive to finally laminated (Figure 18) to deformed and fractured as a result of secondary gypsum growth. Laminated mudstones have thin crinkled laminae that resemble algal stromatolites, and Awramik (this volume) identified algal coccoids and filaments from these laminated rocks. Most of the mudstone is composed of uniform and fine-grained anhedral dolomite crystals in the size range 2 to 4  $\mu\text{m}$ . Sparse and very poorly preserved shells of small pelecypods, ostracodes, and possibly gastropods are scattered through the mudstone. In places the mudstone contains considerable fine-grained organic matter, and a hydrocarbon show was noted in the bottom part of Core 17. Among the laminated mudstones some of the laminae contain abundant clay minerals which give unit extinction under crossed nichols because of the preferred alignment along bedding.

Much of the primary character of these mudstones is disrupted by coarse to fine crystals of secondary gypsum which grew in dolomitic mud. These are scattered throughout the mudstones (Figure 19), and in places

they become so voluminous that they compose most of the rock (Figure 20). The most striking disruptive effects of these gypsum crystals are evident in the laminated mudstones (Figure 21), where their growth has pried layers apart and caused fracturing and folding of layers, the latter process forming small tepee structures in some cases (cf. Horodyski and Vonder Haar, 1975). Much of the secondary gypsum is composed of very large single crystals, up to 2 cm across, and the mudstones are cut in several places by veins of white satin spar.

Many of the large gypsum crystals contain inclusions of two kinds: (1) small euhedral to needle-shaped crystals of anhydrite, that typically occur in descussate clusters, commonly near the centers of gypsum crystals as if forming a core; and (2) irregular patches of dolomitic mud. It is evident that many of the coarse gypsum crystals have replaced anhydrite which probably had formed originally as small displacive nodules (themselves perhaps originally as diagenetic gypsum; Vonder Haar, 1976) within the dolomitic mud. Yet growth of the gypsum crystals apparently extended

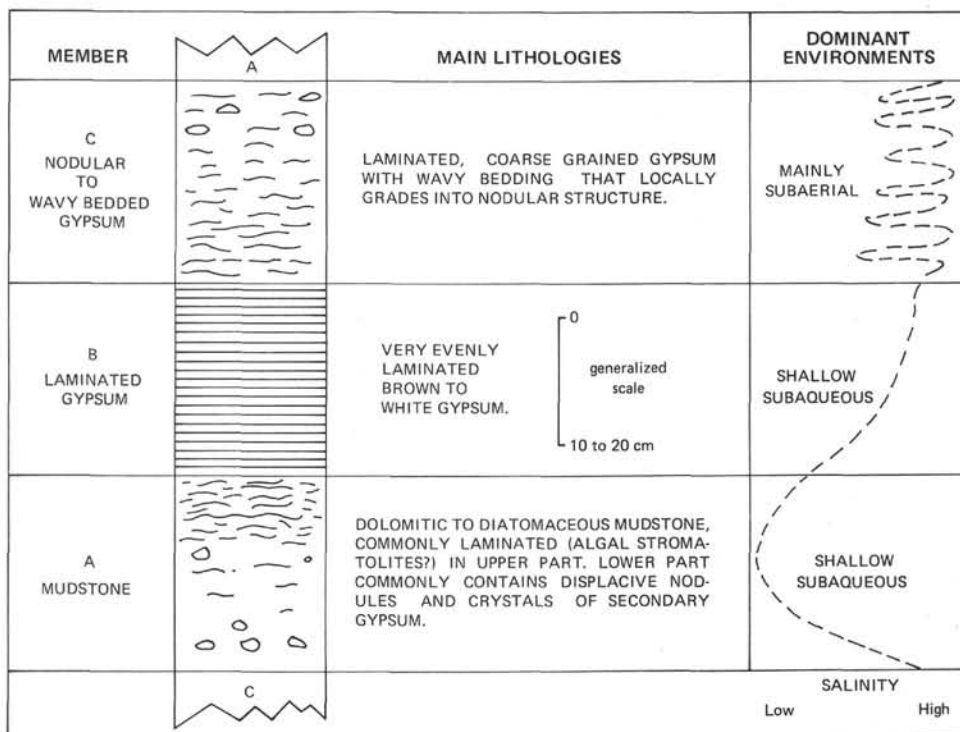


Figure 17. Idealized portrayal of the members of a single gypsum-mudstone cycle at Site 374. The dotted line at right represents a very generalized salinity curve.



Figure 18. Member A of gypsum-mudstone cycle at Site 374, core photograph. This is dolomitic mudstone with laminated algal stromatolites at the bottom. Coin diameter is 1.9 cm (372-17, near the top of the section).

beyond the confines of the anhydrite nodules to shoulder aside the adjacent dolomitic mud, and possibly also to replace portions of this mud.

There is also evidence that some of the gypsum crystals may have filled previously formed cracks. Figures 22(A) and 22(B) show a laminated mudstone with intersecting cracks now filled by a large single, continuous gypsum crystal. The edges of the cracks, however, are lined by small elongated calcite crystals that must have grown into void space prior to precipitation of the gypsum. The latter may have widened the crack, but

the crack itself formed earlier, possibly as a desiccation feature.

Likewise, not all of the brecciation in member A mudstones can be attributed to displacive crystallization. Figure 23 shows clasts of laminated dolomite cemented in a dolomitic matrix. The clasts are rich in organic material and resemble algal stromatolites. This is thus an intraformational breccia formed by erosion and redeposition of possible algal stromatolites.

A further variation is the occurrence of laminated diatomaceous mudstones in Core 17. These contain an estimated 50% to 60% diatoms, the remainder being clay minerals and fine dolomite. According to Schrader and Gersonde (this volume) the diatom species present are restricted, brackish water forms. Por (1972), however, has noted that in hypersaline lagoons and pools bordering the Sinai Peninsula, fresh-water faunal elements become dominant when salinity values exceed 100,000 ppm.

Only Core 17 contained an interval in which both the top and the bottom of member A appear to be exposed (Figure 16), all others containing only partial segments. The A member in Core 17 is 94 cm thick. The contact with the underlying C member seems somewhat transitional. Large displacive gypsum crystals are especially abundant in the lower portion of A member mudstones where they cause considerable disruption. The diatomaceous mudstone occurs near the center of the member. Laminated, stromatolitic mudstones that contain algal coccoids and filaments (Awramik, this volume) occur near the top of the member where the laminae are considerably deformed by secondary displacive gypsum, and where they pass



Figure 19. Member A of gypsum-mudstone cycle at Site 374, core photograph. White areas are secondary gypsum crystals which grew displacively in dolomitic mudstone. Coin diameter is 1.9 cm (372-17, near middle of section).

transitionally within a few centimeters into the very evenly laminated gypsum of the overlying B member. Identical upper contacts of this kind are present in the bottom of Cores 18 and 19.

We interpret the dolomitic mudstones of member A as largely the product of shallow, subaqueous deposition. Analysis of the organic matter in these mudstones suggests marine influences (Deroo et al., this volume). But water depth may have fluctuated considerably, and at times brief intervals of desiccation may have occurred causing cracking (Figures 22[A] and 22[B]) and leading to the formation of sedimentary intraformational breccias (Figure 23). Short-lived episodes of desiccation might also explain the presence of nodular anhydrite and secondary gypsum; a likely source for these would be concentrated pore waters beneath a sabkha. Although not well documented in these cores, there is a suggestion of a regular progression of facies within the A member. Secondary gypsum is most abundant, though not restricted, to the bottom part of the member, diatomaceous mudstone occurs in the center part, and laminated, stromatolitic mudstone is most common at the top. A possible interpretation is that the basal gypsum-rich mudstones represent very shallow subaqueous deposition with periodic subaerial emersions; that progressive deepening and probable freshening of the water culminated in deposition of the diatomaceous mudstone; and that the onset of stroma-

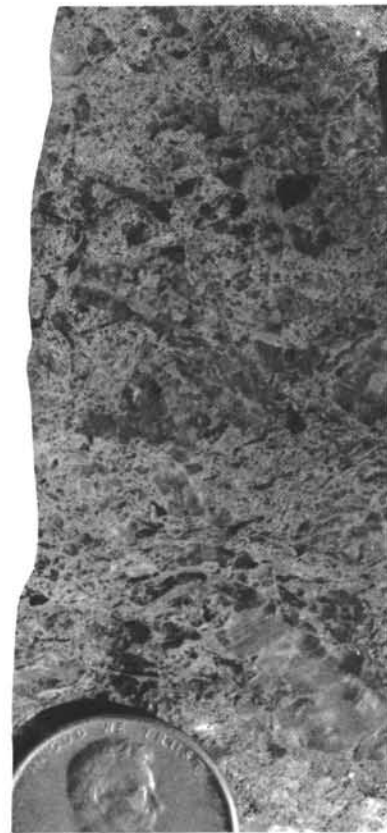


Figure 20. Member A of gypsum-mudstone cycle at Site 374, core photograph. Very high density of secondary, displacive gypsum crystals in dolomitic mudstone near the bottom of member A. Coin diameter is 1.9 cm (372-17, near bottom of section).

tolitic deposition at the top of the cycle records renewed shallowing and possibly increased salinity. Similar algal laminated carbonate sediments with displacive gypsum have been reported in modern hypersaline environments of the Dead Sea (Neev and Emery, 1967), in mudflats bordering Laguna Madre, South Texas (Masson, 1955), in coastal lagoons of Baja California (Horodyski and Vonder Haar, 1975; Vonder Haar, 1976; Horodyski et al., in press), and also in the Miocene Gessoso-Solfifera Formation of Sicily (Schreiber and Freidman, 1976; Hardie and Eugster, 1971) and the Messinian of the northern Apennines (Vai and Ricci Lucchi, in press).

**B Member:** The B member is composed of brown gypsum with white blotches and with even and generally flat laminations. The rock has pronounced parting parallel to bedding that cause it to split into wafer-thin pieces. This is the type of gypsum called "Balatino-nero" by workers in Sicily. The darker laminae tend to be flatter and more even, the lighter ones more irregular and with a somewhat recrystallized appearance. On a megascopic level, some gypsum layers have what

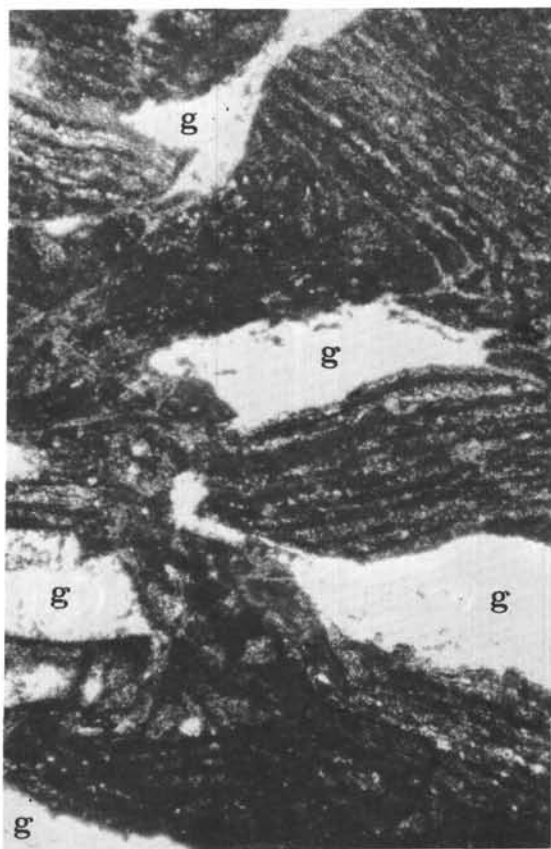
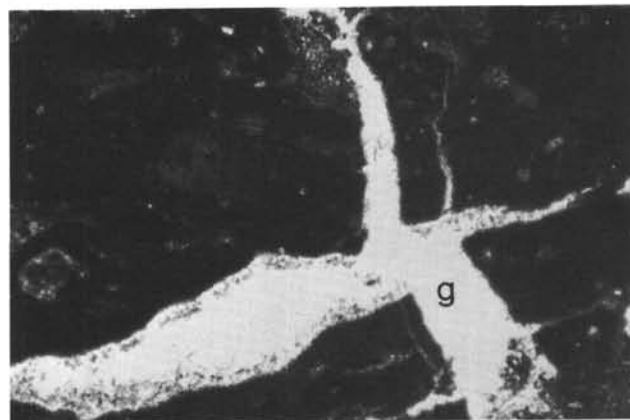
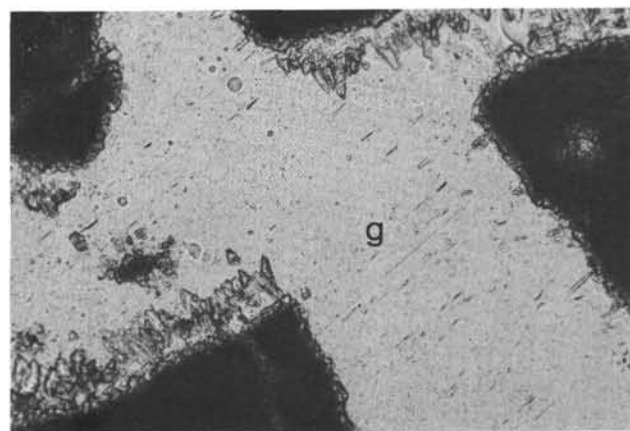


Figure 21. Member A of gypsum-mudstone cycle at Site 375, photomicrograph, plain light. Lenticular, secondary gypsum crystals ("g") grew displacively in laminated dolomitic mudstone and deformed the mudstone. Scale bar is 500  $\mu\text{m}$  (374-18-1, 146-130 cm).



A



B

Figure 22. Member A of gypsum-mudstone cycle at Site 374, photomicrographs, plain light (374-17-1, 92-5 cm). (A) A single crystal of secondary gypsum ("g") fills two intersecting cracks in dolomitic mudstone (dark). Cracks are lined by small crystals of void-filling carbonate (calcite or dolomite?) which predates growth of the gypsum crystal. Scale bar is 500  $\mu\text{m}$ . (B) Enlargement of center part of A. Note that the rim cement of secondary carbonate crystals is thicker and more fully developed on the horizontal crack; this suggests that it formed and began to be filled by carbonate cement earlier than the vertically inclined crack. Scale bar is 200  $\mu\text{m}$ , g = a single gypsum crystal.

appear to be recrystallization crusts and reverse grading like those at Site 372 but much less obvious. Faint and small-scale cross bedding is present in Core 19.

Thin-section observations reveal two important details: first that the gypsum has undergone extensive recrystallization, and second that many of the coarser gypsum crystals contain abundant anhydrite inclusions. The laminae are defined by very thin (ca. 10  $\mu\text{m}$ ), undulating to discontinuous seams of reddish brown organic matter, possibly algal or bacterial coatings. Some of these seams are compound and anastomosing. They separate laminae of gypsum that are 2 to 4 mm thick and have faint micro-laminae defined by wisps of very fine-grained organic material. The most common texture within the gypsum laminae is finely granoblastic, consisting of a rather poorly sorted assortment of irregularly shaped, interlocking gypsum crystals that range in maximum dimension from 10 to about 80  $\mu\text{m}$ . This is a recrystallization texture. But in a few favorable cases, laminae with reversed grading comparable to that at Site 372 can be recognized through the screen of recrystallization. Many of these gypsum laminae contain rather abundant inclusions of fine-grained organic matter which imparts the brown color

to the rock. Slender laths of anhydrite are also rather common in some of these laminae, usually near the top just below the thin organic seam. But they are much more abundant in the coarse gypsum described in the following paragraphs.

Cutting across both the fine granoblastic texture and the thin organic seams are large, relatively clear gypsum crystals of a later replacement generation (cf. Ogniben, 1957; West, 1964). These attain maximum sizes of 700 to 800  $\mu\text{m}$ . Many of these coarse crystals are elongated parallel to bedding and seem to replace some laminae. It is within these coarse crystals that the majority of anhydrite inclusions occur, often as clusters near their centers, as if the coarse gypsum grew poikilolitically around a small anhydrite nodule. The anhy-

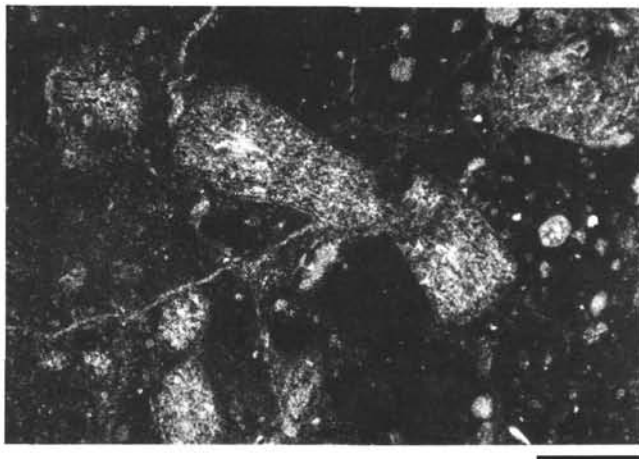


Figure 23. *Member A of gypsum-mudstone cycle at Site 374, photomicrograph, plain light. Clasts of faintly laminated, dolomite rich in organic matter (probably algal stromatolites) rests in dark matrix of dolomitic mudstone. Scale bar is 500  $\mu\text{m}$  (374-17-1, 92-95 cm).*

drite clusters are composed of subhedral to euhedral laths most of which are 30 to 50  $\mu\text{m}$  long and arranged in felted to aligned felted textures.

A still later generation of coarse, clear gypsum crystals is present as thin replacement veins which trend mostly parallel or subparallel to bedding. These veins commonly lie just above or below the thin organic seams which apparently were planes of weakness. The crystals in these veins contain few inclusions, they have relatively straight or slightly curving grain boundaries, and they transect all of the textures and structures described above.

Because pervasive recrystallization has altered many of the primary characteristics of these rocks, we are on less firm ground in our environmental interpretation compared to the laminated gypsum at Site 372. Nonetheless, the gypsum of member B is sufficiently similar to the laminated gypsum of Site 372 and of the Gessoso-Solfifera Formation of Sicily that we feel justified in making comparisons. As in both of these examples, we interpret the laminated gypsum of member B as shallow subaqueous sediments, deposited mainly from currents (cf. Schreiber et al., in press). Judging from the flatness of the laminations and the scarcity or absence of current-formed structures like cross lamination, ripples and rip-up breccia, the environment may have been quieter and perhaps deeper or more protected than that for the laminated gypsum at Site 372. If the thin organic seams are algal Stromatolites, however, it must have lain well within the photic zone. The overall characteristics of this gypsum bear resemblances to that in a protected evaporite flat overlying a former lagoon in the Mormona complex of Baja California (Vonder Haar, 1976).

The effects of later diagenesis have tended to obscure the evidence of the earliest diagenetic phases. On the basis of limited observations, we suspect that many of the laminae had reversed grading like that at Site 372. But the effects were apparently much less drastic

and did not result in the wavy bedding characteristic at that site. Many details of the later phases of diagenesis remain unclear to us, but the major events must have included at least the following:

- 1) Formation of the finely granoblastic gypsum mosaic, perhaps by recrystallization of the primary gypsum fabric or of a precursor fabric formed even earlier during diagenesis.

- 2) Formation of the anhydrite laths in nodules or layers. This may have occurred before, during or after event (1) above—the textural evidence is equivocal. We suspect the anhydrite formed relatively early during diagenesis by replacement of gypsum (cf. Gavish, 1974; Orti Cabo and Shearman, in press). The fact that anhydrite is common near the tops of gypsum laminae suggests its formation was rhythmic and possibly related to rhythmic variations in salinity of the overlying water which in turn affected pore waters.

- 3) Replacement of granoblastic gypsum and felted anhydrite layers by coarse gypsum. The anhydrite-rich layers were preferentially replaced, with small anhydrite nodules perhaps serving as nuclei which the large gypsum crystals enveloped. We are uncertain what caused this replacement; the problem is discussed further in the following section.

- 4) Formation of thin gypsum veins by replacement and by precipitation in cracks parallel to bedding.

This postulated sequence invites comparison with the diagenetic stages reconstructed by West (1964) through careful petrographic study of Purbeckian evaporitic rocks in Britain. In particular, event (3) above appears to correlate with West's Stage IV or V.

**C Member:** The most common lithology in Cores 16 to 20 is brown to white, wavy bedded to nodular gypsum which constitutes the C member of the cycle. Intervals of this lithology that are 80 and 130 cm thick occur respectively in Cores 16 and 20, and thinner intervals are present in Cores 17, 18, and 19. Very commonly, bands, 2 to 10 cm thick, of coarse, crudely layered or structureless gypsum that appears highly recrystallized, alternate with bands of similar thickness that are composed of somewhat finer gypsum with wavy bedding and darker hues (Figure 24). Scattered throughout both kinds of bands, but more common in the former, are small blebs, nodules, and irregular to discontinuous layers, of white gypsum (Figure 25). This white gypsum cuts all other fabrics and appears to be a later stage replacement. In places rather coarse crystals of more or less randomly oriented selenitic gypsum form bands a few centimeters thick.

The observations above suggest a complex sedimentary and diagenetic history, and this is confirmed by microscopic study. The basic structures of the wavy bedding are gypsum laminae, 2 to 8 mm thick, separated from each other by thin anastomosing fine carbonate seams, commonly very rich in organic matter and very irregular. Most of the gypsum is a granoblastic mass of coarse-grained crystals, clearly a recrystallization texture. Many of the laminae show a distinct polarity, with the bottom composed of relatively clear and inclusion-free gypsum, and the upper parts by

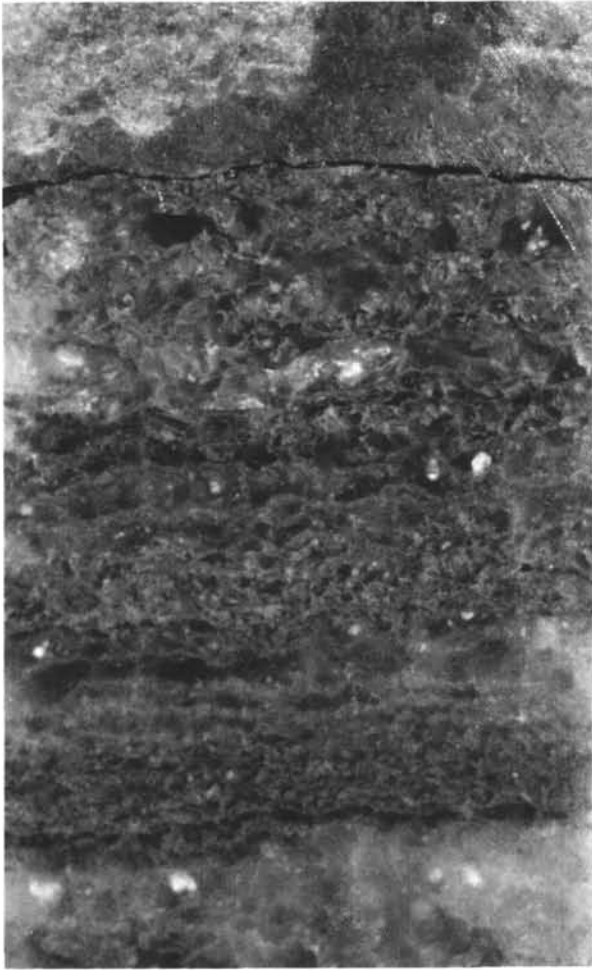


Figure 24. Member C of gypsum-mudstone cycle at Site 374, core photograph. Laminated gypsum shows variation from wavy bedding near center of photograph to coarsely crystalline near the top and bottom. Scale bar is 1 cm (374-20-1).

cloudy gypsum with abundant inclusions of anhydrite laths and fine-grained carbonate and organic matter (Figure 26).

As in the other members of these cycles, diagenesis of the calcium sulfate minerals has been complicated and has produced various overprintings (Figure 26) which tend to obscure primary textures as well as those formed during the earlier stages of diagenesis. In a few thin sections, however, enough vestiges of earlier textures can be recognized to allow at least a rough reconstruction of events. For example, the clear basal parts of a few laminations contain elongated selenitic gypsum crystals, some of them having swallow-tail twins oriented perpendicular to bedding. This texture suggests growth on the bottom of a brine pan, but most commonly these crystals lie with their long axes parallel or subparallel to bedding or they occur in randomly oriented piles, suggesting reworking due to dissolution and/or to current action following their growth.

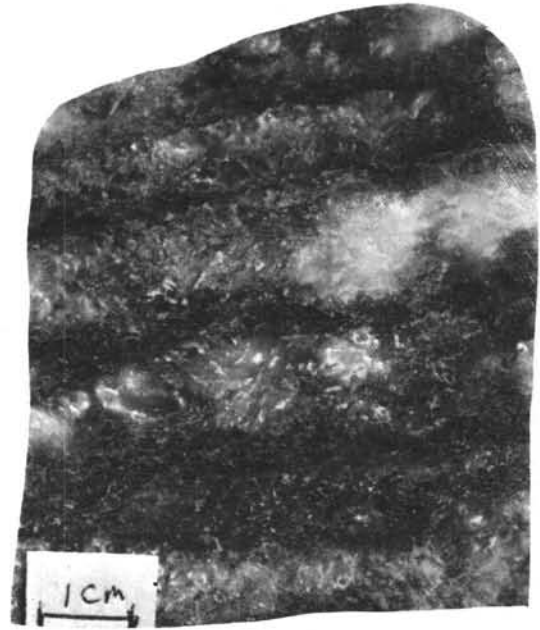


Figure 25. Member C of gypsum-mudstone cycle at Site 374, core photograph. Laminated gypsum with wavy bedding and small blebs and nodules of secondary gypsum (white) (374-18-1, 123-127 cm).

The top parts of some of the millimeter-thick laminations consist of very coarse gypsum in which trains of fine-grained anhydrite and carbonate inclusions record crystallographic planes within former crystals. These were doubly terminated, and we believe they were idiomorphic quartz (Tarr, 1929; Grimm, 1962b), now replaced by a later generation of coarse gypsum (Figures 27, 31[A], and 31[B]). The long axes of these ghost crystals are usually oriented perpendicular or at high angles to bedding, and often they are surrounded by thin pockets of micritic carbonate which appears to have been squeezed by their growth. Most of these ghosts have included anhydrite laths and small amounts of celestite in patches that lie at or near their centers. We interpret these ghosts as diagenetic quartz crystals which grew displacively within soft sediment composed of micritic carbonate and anhydrite, the latter possibly as small nodules around which the quartz grew. In some cases the crystals may have protruded slightly above the sediment surface. The upper parts of many of these ghost crystals have been dissolved (Figure 27) by post-burial stylolitic solution after gypsum had replaced the quartz.

Some of the gypsum laminae lack the polarity of clear-cloudy gypsum described above and consist instead of crudely layered thin bands of micritic carbonate which form semirounded enclosures around coarse gypsum crystals, a structure that resembles chicken wire structure on a microscopic scale (Figure 28). Most of the gypsum crystals extend through several of the intercarbonate areas. Most of them also contain abundant anhydrite inclusions, and in some instances the

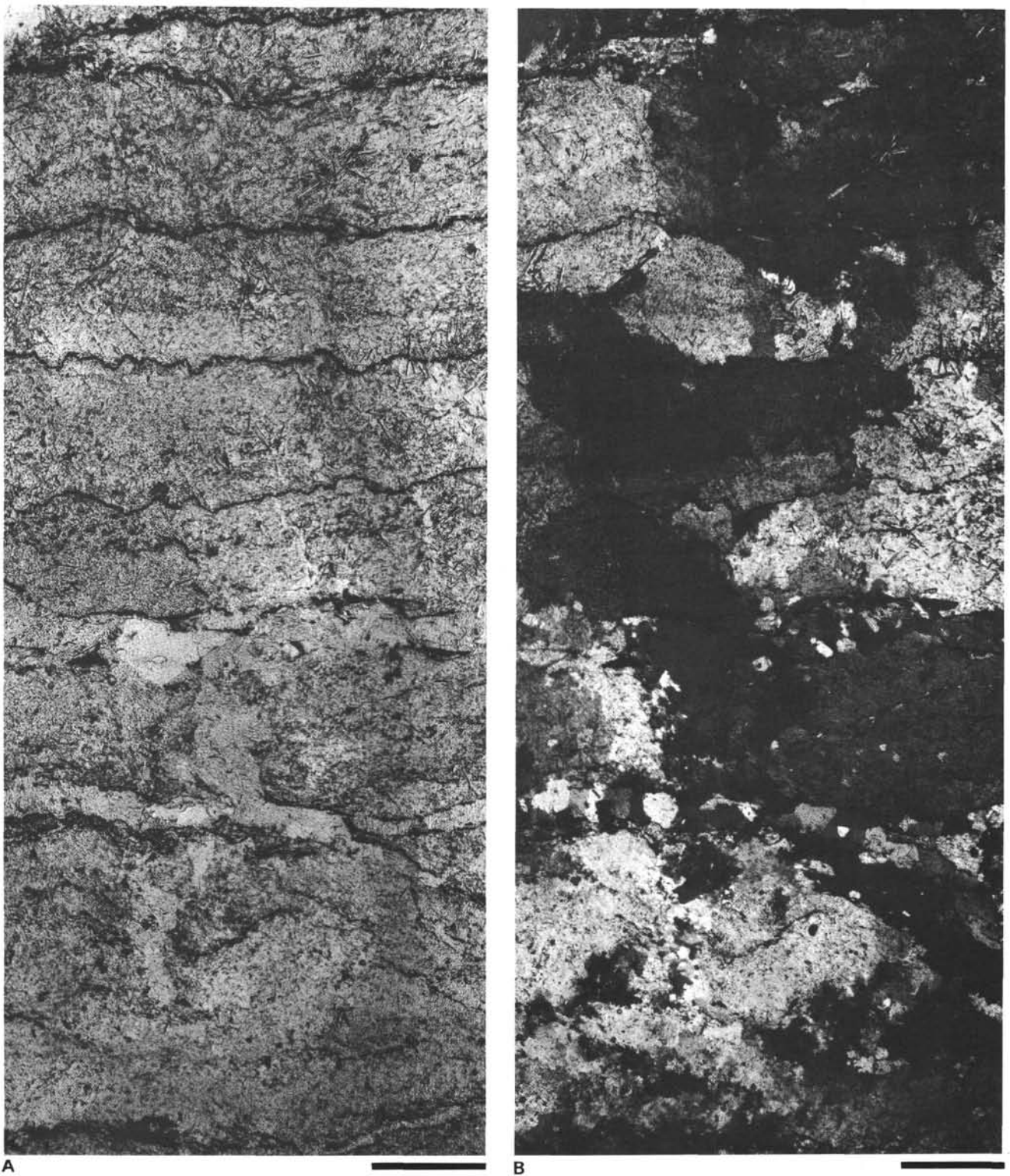


Figure 26. Member C of gypsum-mudstone cycle at Site 374, thin-section photograph. Photo A is plain light, B is partly crossed nicols. Laminated gypsum with coarse recrystallization mosaic. Undulating, organic matter-rich seams (thin dark lines in photo A) serve to define the laminations. The needle-like crystals in the gypsum are inclusions of anhydrite laths (best seen in photo A). Note, in photo B, how the coarse gypsum crystals of the recrystallization mosaic cut across all earlier fabric elements. A small gypsum-filled vein occurs in the bottom half. Scale bars are 2 mm (374-20-1, 134-136 cm).

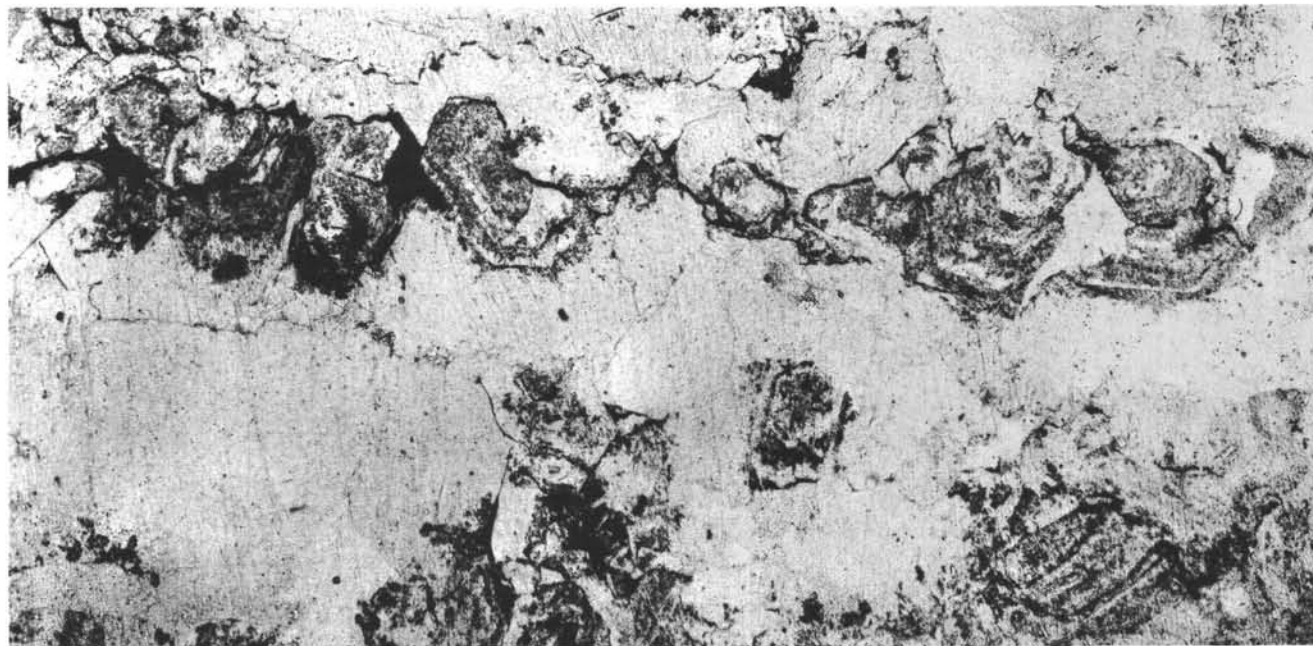


Figure 27. *Member C of gypsum-mudstone cycle at Site 374, thin section photograph, plain light. Laminated gypsum in which thin, dark stylotitic seams define the lamination. All of the rock has been recrystallized to a coarse mosaic of gypsum (cf. Figure 26). The euhedral crystal outlines are of idiomorphic, secondary quartz which a later generation of gypsum has replaced (cf. Figure 31). Crystallographic faces are defined by inclusions of anhydrite laths and micrite. Note how the stylolites truncate the pseudomorphed crystals. Scale bar is 2 mm (374-16-1, 114-117 cm).*

intercarbonate areas are about half anhydrite inclusions, half poikilitic gypsum. We interpret these as small anhydrite nodules which grew displacively in a carbonate mud, but were later partly replaced by coarse gypsum. The actual history may be a good deal more complex. For example, in a few sections we noted what appear to be two generations of anhydrite (Figure 29), one composed of small laths 10 to 100  $\mu$ m long, the other of relatively coarse euhedral ones up to 600  $\mu$ m in length. Instead of single crystals, some of these nodular bodies consist of fine alabastrine gypsum; in the experience of one of us (C. S.) this texture commonly develops when gypsum replaces anhydrite laths (see also Vai and Ricci Lucchi, in press). Within the same thin sections, however, the alabastrine gypsum is partly being replaced by coarser mosaic gypsum. Thus, we may have recognized only a few of many stages of mutual replacement between anhydrite and gypsum (cf. Ogniben, 1957; West, 1964). Orti Cabo and Shearman (in press) have described somewhat similar sequences of mutual replacement between gypsum and anhydrite.

Among the other primary features noted are trains of brine shrimp eggs enclosed in coarse selenitic gypsum; these are best developed at Site 378, and we describe them in detail in our discussion of selenitic gypsum there. Among the diagenetic features are: (1) small clots of fibrous, length slow chalcedony (lutecite) which replace portions of the secondary gypsum; (2) veins of clear gypsum (Figure 26), and (3) laminae rich in organic matter which are the residue of stylotitic seams (Figure 27). Although included anhydrite laths commonly form cores for later poikilitic gypsum crystals,

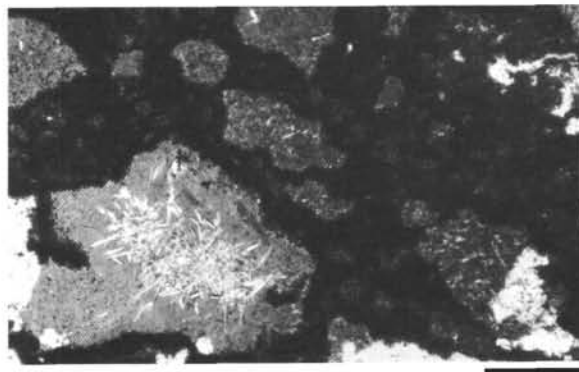


Figure 28. *Member C of gypsum-mudstone cycle at Site 374, photomicrograph, plain light. Nodular gypsum. Irregularly shaped nodules (light gray) are actually single crystals of gypsum that contain numerous inclusions of small anhydrite laths. The nodules reside in dark, fine-grained dolomite. White areas are artifacts in the thin section caused by plucking. We surmise that the gypsum crystals replaced small nodules of anhydrite. Scale bar is 500  $\mu$ m (374-20-1, 134-136 cm).*

many such laths also are concentrated along crystal boundaries between crystals of the last generation of gypsum.

Our interpretation of member C is that its depositional environment varies from very shallow subaqueous to subaerial, and that most of the laminations comprise "minicycles" which reflect this variation. Figure 30 portrays schematically the major stages of a minicycle and the resulting products (cf. also West,



Figure 29. Member C of gypsum-mudstone cycle at Site 374, photomicrograph, crossed nicols. Euohedral inclusions of anhydrite, dolomite, and celestite in coarse crystals of secondary gypsum. Note two distinct sizes of anhydrite inclusions. Scale bar is 500  $\mu$ m (374-20-1, 101-105 cm).

1964). Stage 1 is subaqueous precipitation of small selenite crystals on the bottom of a shallow brine pan. Other kinds of gypsum may have been deposited as well during Stage 1, either along with selenite or without it; these include suspension settled gypsum needle precipitates or mechanically transported gypsum crystals. During Stage 2 the selenite is eroded and redeposited into piles, either by subaqueous erosion or during the early phases of subaerial exposure. Carbonate sediment and possibly additional gypsum is formed during the last phases of subaqueous deposition; and it is within the upper few millimeters of this sediment that anhydrite grows displacively during the subaerial exposure of Stage 3, probably by replacing previously formed gypsum in the presence of very warm, highly concentrated brines. Stage 4 is resubmergence by fresher waters of probable lower temperatures just prior to the onset of a new minicycle; among the consequences are: (1) the formation of idiomorphic quartz crystals that partly replace the anhydrite nodules, and (2) the possible growth of algal mats at the sediment-water interface. The minicycle thus involves fluctuations in both water level and the salinity of the fluids which affect the sediments. We may surmise that the replacement of anhydrite by idiomorphic quartz occurred in sulfate-rich and possibly very alkaline pore waters (cf. Schaller and Henderson, 1932; Stewart, 1951; Grimm, 1962a, b; West, 1964; Folk and Pittman, 1971; Siedlecka, 1972). The ultimate source of the silica could have been dissolution of diatom frustules deposited in mudstone of the A member or perhaps trapped in the thin algal mats within the C member.

We should emphasize that these stages are highly idealized and do not explain every lamina in member C. Among the significant variations are laminations composed entirely of partly replaced anhydrite nodules (Figure 28) and layers in which anhydrite inclusions are distributed rather evenly through the laminae

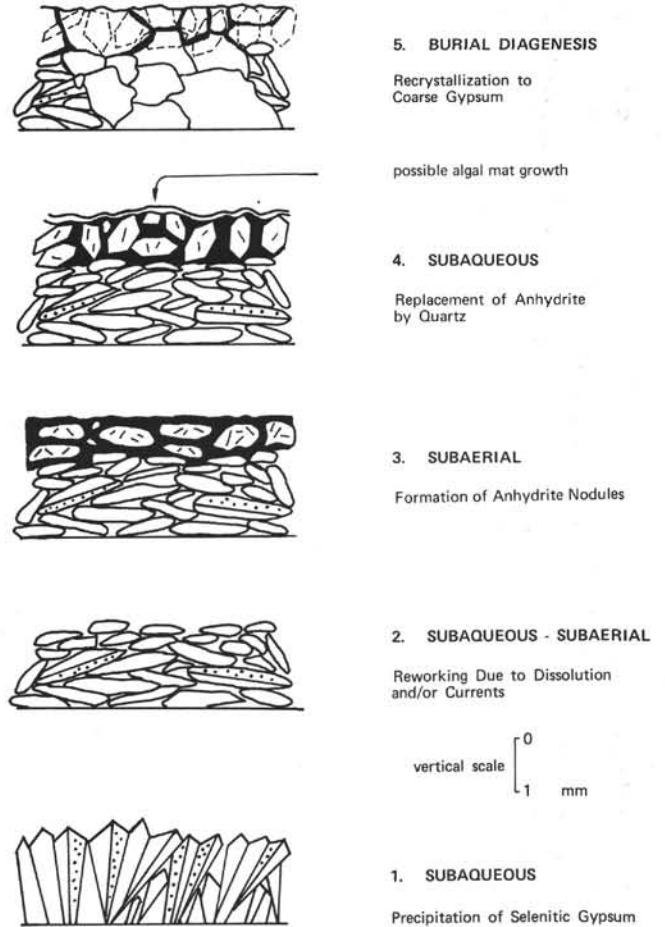


Figure 30. Schematic portrayal of important sedimentologic and diagenetic events in the development of "minicycles" in member C of the gypsum-mudstone cycles at Site 374. See text for discussion.

(Figure 26). Formation of these laminae probably occurred entirely during subaerial exposure.

Stage 5, strictly speaking, is not part of the minicycle, but occurs much later during burial diagenesis. One effect is stylolitic dissolution of secondary gypsum crystals along seams rich in organic matter. The major effect, however, is recrystallization into a very coarse gypsum mosaic that cuts across all earlier formed textures and structures, including stylolites (Figures 26 and 31). We are uncertain of the origin for this recrystallization but the fabrics thus produced resembles coarse recrystallization fabrics in some metamorphic rocks. This stage appears to correspond to Stage IV or V of West (1964).

#### Interpretation of the Cycle in Cores 16-20

Cores 16 through 20 contain parts of at least five ABC cycles, the average thickness of the complete cycle being between 1 and 3 meters. They resemble very closely Messinian cycles described in Sicily (Richter-Bernburg, 1973; Heimann and Mascle, 1974; Schreiber, 1974; Schreiber et al., in press) and in the Ionian Islands (Braune et al., 1973; Fabricius et al., this volume). Coring at Site 132 on the Tyrrhenian Rise during Leg 13 recovered parts of what appear to

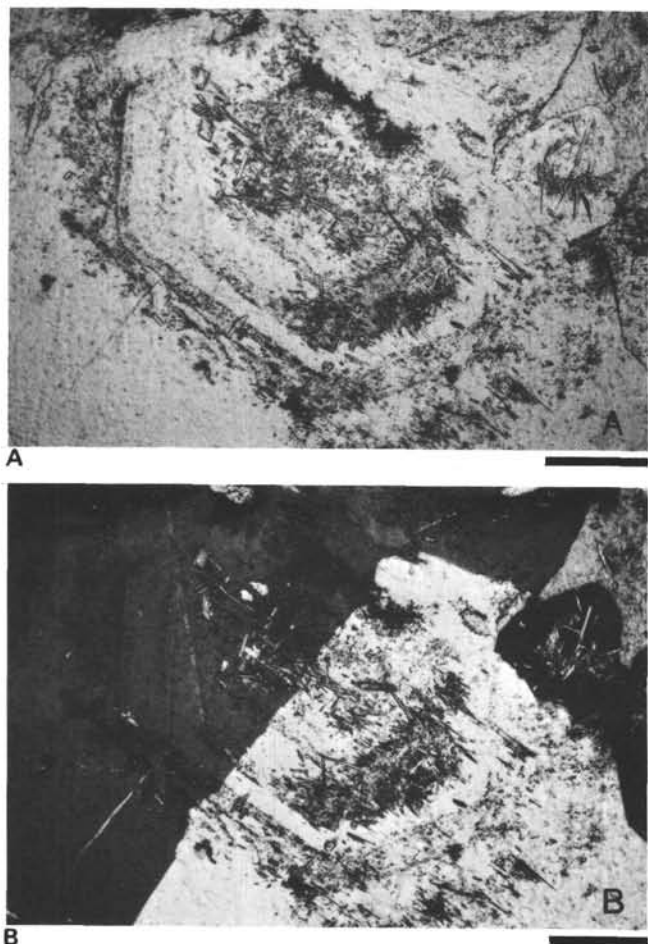


Figure 31. Member C of gypsum-mudstone cycle at Site 374, photomicrograph; photo A is plain light, B is crossed nicols. Trains of inclusions (anhydrite and mirrite) outline the crystal faces of an idiomorphic quartz crystal which apparently replaced anhydrite. Coarse secondary gypsum crystals, in turn, replaced the quartz, and grew across its crystallographic planes (photo B). Scale bars are 500  $\mu\text{m}$  (374-16-1, 114-117 cm).

be similar cycles marked by extensive diagenesis of calcium sulfate sediments (Ryan, Hsü, et al., 1973; Nesteroff, 1973a; Friedman, 1973). Our reconstruction of the events within each of the members of the cycle suggests that the change from member A through B to C records a general lowering of water level, increasing salinity and increasing degrees of subaerial exposure (Figure 17). The overall cycle therefore is one of submergence-desiccation, as a result of flooding and subsequent evaporation. In our interpretation, the A member represents the most continuously submerged period of deposition, B reflects mostly subaqueous deposition but in water of heightened salinity, and C records the predominant influence of subaerial exposure and very saline pore waters.

We must emphasize, however, that this is the general trend, and that short-term fluctuations were superimposed on this trend. Thus, for example, there is evidence for subaerial exposure in all three members of

the cycle, even though subaerial diagenesis was clearly more important during formation of the C member. Episodes of subaerial exposure during deposition of the A and B members were undoubtedly brief.

The range of features in these cycles resembles very closely those found in Holocene tidal flat cycles of arid regions, e.g., those beneath sabkhas of the Trucial Coast (Butler, 1970). In a tidal flat setting, the brief episodes of subaerial exposure during deposition of the A and B members might represent very low tides, conversely the subaqueous phase in C would represent very high tides. In the tideless sea of a desiccating Mediterranean, they could, on the other hand, correspond to slight fluctuations of climate or marine influx that raised or lowered water level over rather short time spans, e.g., a few years or a few tens of years. The laminations, most prominent in members B and C, probably record short-term climatic fluctuations or regional storms with high wind velocities, causing attendant slight shifts in water level. The possibility that such slight fluctuations of water level could produce these sedimentological changes suggests that water depth was very slight and that the basin floor was extremely flat. The situation was thus perhaps analogous in many ways to the epeiric sea model formulated by Irwin (1965) and Shaw (1964) in which only slight changes (e.g., in water level) trigger very widespread facies changes.

For the cycle as a whole, the record of changes in water level and salinity suggests longer term climatic changes of major magnitude, possibly associated with fluctuations in late Miocene glaciation (Bandy et al., 1969; Kennett and Watkins, 1974).

#### Layered Anhydrite and Halite of Cores 21 and 22

More saline phases appear below the gypsum-mudstone cycles just described. Anhydrite constitutes the total 50 cm recovery of Core 21 and the top 78 cm of Section 1, Core 22. Below this is 335 cm of halite in the bottom part of Section 1 and in Sections 2 and 3 of Core 22.

The 50 cm of anhydrite in Core 21 are brown to gray and have a few thin interlayers of soft gray dolomitic mudstone. The anhydrite in Section 1 of Core 22 is mainly white with thin dark interlayers and closely resembles the anhydrite in Core 8 at Site 371 and in Cores 8-13, Site 124 of Leg 13 (Ryan, Hsü, et al., 1973; Nesteroff, 1973a; Friedman, 1973). Nearly all of the anhydrite at Site 374 is layered, but locally it becomes nodular, with the development of small-scale chicken wire structure (Figure 32). The layering consists chiefly of anhydrite laminae, a few millimeters to two centimeters thick, bounded by thin undulating, anastomosing or discontinuous seams of dark organic matter or organic matter-rich, fine grained, dolomite. Considerable variation exists in the thicknesses and degree of irregularity of the laminae. The thicker laminae of white anhydrite in Core 22 seem to be formed of coalesced small nodules. In the classification of Maiklem et al. (1969), the main structures are termed bedded mosaic and distorted bedded mosaic.

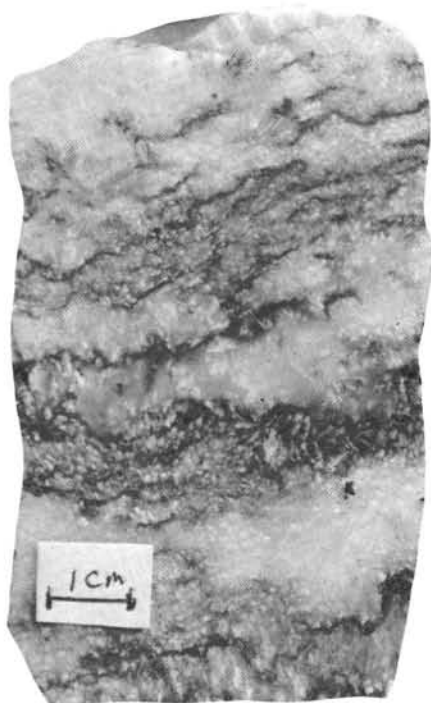


Figure 32. *Laminated to nodular anhydrite at Site 374, core photograph. Small white blebs are areas of secondary replacement by gypsum (374-22-1, 58-65 cm).*

Throughout the anhydritic interval are small halite-filled areas up to 1 cm across (Figure 33). They vary considerably in shape but many are somewhat elongate parallel to bedding. In thin section many of these patches can be seen to contain, in addition to halite, rims of rather coarse (up to several hundred microns long) euhedral anhydrite laths that appear to have grown into void space. There are also a few small patches composed entirely of this coarse anhydrite. The halite and most of the anhydrite of these rocks probably originally were formed contemporaneously, the halite being precipitated as crystals or clusters of crystals in an anhydritic mud. Subsequently, however, some of the halite must have dissolved creating small vugs into which anhydrite crystals grew. A later generation of halite precipitated in those vugs not completely filled by secondary anhydrite.

Microscopically, most of the anhydrite is densely packed small laths with felted texture, and it contains scattered patches of fine-grained organic matter. The white anhydrite of Core 22 has local replacement of anhydrite by gypsum. Megascopically, this can be visible as small white, soft blebs (Figure 32). Microscopically the gypsum, present as masses of tiny acicular crystals, replaces the small anhydrite laths but not the later-stage coarse crystals.

Along with the anhydrite at Site 371, the anhydrite at Site 374 resembles anhydrite nodules now forming beneath Trucial Coast sabkhas (Kinsman, 1969; Butler, 1970) and is identical to numerous ancient exam-

ples likewise attributed to the sabkha environment (e.g., Shearman and Fuller, 1969; Fuller and Porter, 1969; Shearman, 1971; Friedman, 1973; Bebout and Maiklem, 1973; Stoffers and Kuehn, 1974). In all these examples the thin organic matter-rich partings between anhydrite masses are interpreted as the remains of algal mats squeezed aside during displacive growth of anhydrite.

The halite of Core 22 is translucent and colorless to gray. It contains thin, gray, irregularly shaped interlayers of fine-grained polyhalite as well as scattered inclusions of this material. In some parts of the core the interlayers are spaced a few millimeters apart, in other parts they are separated by up to 10 cm of relatively pure halite. In places, particularly in Section 2, there is considerable distortion of the polyhalite interlayers, some of which dip vertically. We attribute this deformation to diagenetic recrystallization of halite.

R. Kuehn has discovered bittern salts associated with halite in Section 3 of Core 22 (Kuehn and Hsü, this volume). In addition to polyhalite  $[K_2MgCa_2(SO_4)_4 \cdot 2H_2O]$ , rare sulphoborite  $(HMgBO_3 \cdot 2MgSO_4 \cdot 7H_2O)$  occurs with halite between 24 and 30 cm in Section 3. The interval between 107 and 130 cm contains kainite  $(KMgClSO_4 \cdot 3H_2O)$  in addition to



Figure 33. *Anhydrite at Site 374, core photograph. Small, irregularly shaped areas are halite-filled vugs. Structure of anhydrite here is distorted bedded mosaic. Coin diameter is 1.9 cm (374-22-1).*

halite and polyhalite. Sylvite (KCl) and bischofite ( $\text{MgCl}_6 \cdot 6\text{H}_2\text{O}$ ) have also been identified in Core 22.

The recrystallization noted above appears to have destroyed much of the primary fabrics in the rock. Some of the halite crystals, however, appear to have grown as displacive cubes in a calcium sulfate mud. across; based on modern occurrences of polyhalite aggregated into ellipsoidal bodies 150 to 500  $\mu\text{m}$  across; based on modern occurrences of polyhalite (Holser, 1966), we may surmise that it is an early diagenetic replacement of a gypsiferous mud. This is the material which composes the thin, gray interlayers, and in places it contains considerable dark brown organic matter. It also occurs as small intercrystalline patches in the more nearly pure halite layers.

Core 22 also contains some interlayers of halite crystals with chevron structure and laminae composed of well-sorted and rounded, sand-size grains of alabastine gypsum. In some cases, the halite crystals appear to have grown displacively in the gypsum sand. In other cases, the tops of the chevron crystals are very irregular and corroded appearing, suggesting periodic partial dissolution of the halite.

Cores 23 and 24 penetrated subbottom depths from 444.5 to 457 but there was no recovery. Presumably this interval consists of soluble salts that dissolved during coring and/or during retrieval of the core to the ship.

As noted earlier, we interpret the layered anhydrite as the product of early diagenetic displacive crystallization in a sabkha environment. The presence of chevron structures and the rapid variations of bromine content in short stratigraphic intervals suggests halite precipitation in shallow brine pools, and the relatively high bromine content suggests derivation from a marine source (Kuehn and Hsü, this volume). On the basis of their association with the subaerial to shallow water deposits stratigraphically above, we assume the halite and bittern salts were formed in shallow water or subaerially during a hypersaline stage. Possibly these environments were similar to the subaerially exposed evaporite flats in Baja California (Phleger, 1969; Shearman, 1970), which contain halite with thin gypsum interlayers, the latter locally replaced by polyhalite (Holser, 1966). Perthuisat (1971, 1974, 1975) also has described polyhalite associated with halite within a continental sabkha in northern Tunisia.

#### Overall Interpretation of the Messinian Evaporite Sequence at Site 374

The upward change from predominantly halite (Core 22) to anhydrite (Cores 21 and 22) to gypsum-mudstone cycles (Cores 16-20) to dolomitic mudstones (Cores 12-15) records progressive decreases in overall average salinity. The dolomitic mudstone probably also records deepening of the average water depth during a 'Lac Mer' stage, but very shallow and even subaerial environments persisted at least through the deposition of the gypsum-mudstone cycles. On the basis of comparisons with large-scale cycles in the Gessoso-Solfifera

Formation of Sicily (Decima and Wezel, 1973; Schreiber et al., 1976), we surmise that coring at Site 374 penetrated part of one halite to marlstone cycle and that further coring would have encountered additional cycles of this kind.

#### SITE 375, FLORENCE RISE, WEST OF CYPRUS

Discontinuous coring at Site 375 resulted in only sporadic recovery of Messinian evaporitic sediments between subbottom depths of 137 to 194.5 meters. These are of five kinds in their stratigraphic order, from top to bottom: (1) dolomitic marl, (2) selenitic gypsum with thin marlstone interlayers, (3) interlayered gypsarenites, gypsrudites, and finely laminated, light colored gypsum, (4) gray to black, finely laminated gypsum, and (5) dolomitic caliche breccia. These are described and discussed below.

1) Dolomitic marl: This sediment is gray to green dolomitic marl containing nannofossils, ostracodes, and scattered gypsum crystals. Only 2 cm were recovered, in Section 1 of Core 1.

2) Selenitic gypsum with thin marlstone interlayers: This type of material was recovered in Core 1 (90 cm), and in Sections 1, 2, and the top 38 cm of Section 3 of Core 2. The major component is coarse, elongated crystals of selenitic gypsum. These are up to 8 cm long and commonly oriented with elongation perpendicular or at high angles to stratification (Figure 34). Swallowtail twins are common, and some of the crystals are prominently zoned. The crystals vary from fairly clear and translucent to milky, and from very light gray to yellowish and greenish gray.

This gypsum varies also from tightly packed aggregations of nearly pure gypsum to gypsum crystals embedded in greenish gray, sandy marlstone. A few thin interlayers of the latter sediment also occur.

Most of the selenite crystals appear to have grown upward as elongated crystals that sometimes shouldered marly sediment aside through displacive crystallization. Other intervals of the selenite, however, consists of piles of randomly oriented elongated selenite



Figure 34. Selenitic gypsum at Site 375, core photograph. Coarse selenite crystals in marl. Scale bar is 1 cm (375-1-1, 61-66 cm).

crystals, or aggregations of broken, irregularly shaped selenite crystals. We interpret these as reworked layers.

Microscopic observations shed light on these processes of selenite growth and reworking. Many of the coarse selenite crystals contain apparent pellets and eggs of brine shrimp (described in more detail in the discussion of Site 378 in this chapter) suggesting that the crystals grew subaqueously, but in a very shallow-water environment. Some inclusions of celestite are also present. A common fabric consists of clusters of large upright selenite crystals with some intercrystal areas filled by micritic sediment or aggregations of smaller, irregularly shaped selenite crystals or both. We believe the aggregations of smaller selenite crystals result from solution collapse. Some layers consist entirely of such slightly reworked crystals, which show no signs of abrasion and appear to be products of partial dissolution and collapse more or less in place. The same processes seem to have affected the selenite at Site 378, and we discuss this further in a separate section near the end of this chapter.

The interselenite marlstone and marlstone interlayers vary from uniform and even grained to sandy and poorly sorted. Among the sand size fragments identified, abraded gypsum grains are most common, but a variety of terrigenous grains is also present. These include quartz, plagioclase and potassium feldspar, pyroxene, green, pleochroic hornblende, and serpentine. Other components include ostracodes and benthic and planktonic foraminifers, all of which are altered and appear reworked.

Similar selenitic gypsum occurs in Messinian and Pleistocene sequences of Sicily and has been interpreted as subaqueous (Hardie and Eugster, 1971; Richter-Bernburg, 1973; Schreiber and Kinsman, 1975). Goto (1967) has described selenite growth in Australia in shallow lagoons, isolated arms of the sea, and inland depressions fed by seepage of saline ground waters. Perthuisot (1974, 1975) reported selenite forming in a continental sabkha in Tunisia. Most workers have portrayed this as a shallow water form of gypsum, and the presence of pellets and eggs of brine shrimp in selenite at Site 375 tends to support this interpretation. In addition, at Site 375 we take the presence of the dissolution breccias as possibly indicative of periodic freshenings which partially dissolved and undermined vertically growing selenite crystals.

3) Interlayered gypsarenites, gypsrudites, and laminated gypsum: The dominant deposits of this assemblage are clastic layers consisting mainly of angular sand to gravel size particles of reworked gypsum. This grouping of lithologies occurs in the bottom 112 cm of Section 3 and the top 25 cm of Section 4, Core 2.

The clastic arenites and rudites are poorly sorted mixtures of particles of varied kinds of gypsum, including laminated and selenitic varieties, in a fine-grained matrix of micrite. Other components include clasts of marlstone and soft white nannofossil chalk, and detrital quartz and feldspar as well as dolomite of undetermined origin. These components are redeposited but

we found no sedimentary structures diagnostic of a particular depositional mechanism or environment. In a few places coarse secondary gypsum crystals appear to have grown within the sediment.

Interlayered with these coarse clastic units are several thin beds of finely laminated, gray gypsum, the thickest bed being 12 cm. The tops of several of the laminated units are erosionally truncated by the overlying clastic layers. In thin section the laminae consist of normally graded layers a few millimeters thick (Figure 35). The basal part is a coarse-to-medium-grained recrystallization mosaic, and this grades very gradually upward into finer grained gypsum composed of somewhat elongated crystals, or, in some instances, eventually into micritic limestone. We interpret these laminae also as redeposited layers of fine-grained, clastic gypsum.

4) Gray to black laminated gypsum: This sediment was recovered in the bottom 126 cm of Section 4 and the top 5 cm of Section 5, Core 2. The top part of the interval is somewhat lighter colored, the bottom is darker and contains more organic material. None of the laminations, however, have the appearance of algal stromatolites. The millimeter thick laminae appear to have varied structures and origins. Some are normally



Figure 35. Laminated gypsum at Site 375, thin-section photograph, partly crossed nicols. Note that most laminations, bounded by thin dark seams, show normal size grading. Scale bar is 2 mm (375-2-3, 91-95 cm).

graded laminae which appear to be redeposited units like those previously described. Other laminae are composed of couplets (Figure 36) consisting of: (1) a lower sub-lamina composed of relatively coarse-grained gypsum crystals that seem to have grown upward from the sea floor; the tops of these, however, most commonly are planed off by dissolution; and (2) an upper fine-grained sub-lamina containing numerous oriented, elongated gypsum crystals that are characteristic of precipitation at the air-water interface (see discussion under Site 376 of this chapter). This upper part of the couplet was probably current deposited, and in some cases currents also eroded and reworked the basal crystals growing on the sea floor. In a few places, there are also thin cross-laminated intervals. Much of this gypsum has small cross-cutting clayey



Figure 36. Laminated gypsum at Site 375, photomicrograph, partly crossed nicols. Laminae in this specimen consist of alternations of two kinds of sub-laminae. One kind is composed of small selenite crystals, mostly elongate perpendicular to bedding. The other consists of finer grained gypsum crystals, many of which are elongated parallel to bedding (upper part of photo; cf. Figures 45A and 45B). We interpret these as products of in situ growth of selenite alternating with reworking and redeposition of clastic gypsum. Note that selenite crystals forming sub-laminae in the lower half of photograph have blunted crystal terminations, probably due to dissolution. Scale bar is 2 mm (375-2-4, 53-57 cm).

seams that impart a nodular or flaser appearance to the rock. Possible resedimented flat clasts of this laminated gypsum occur in Section 4 between 70 and 77 cm.

5) Dolomitic caliche breccia: Section 5 of Core 2 contains 17 cm of breccia composed of dolomitic lithoclasts, peloids, badly altered biogenic fragments, and coated grains. Some of the dolomitic lithoclasts contain poorly preserved Miocene planktonic foraminifers; among these, M. B. Cita has identified *Orbulina* and *Globigerinoides*. Very similar dolomitic rocks occur in the core-catcher sample of Core 3 and at the top of Core 4. We believe these rocks occur at the base of the evaporite section at this site, and that they are dolomitized caliche breccias formed during subaerial exposure and diagenesis. We discuss this diagenesis more fully under Site 378 where a nearly identical dolomitic breccia occurs. Some rocks in the Calcare di base in Sicily also somewhat resemble these breccias (Ogniben, 1963; Schreiber, 1974).

#### Interpretation of the Messinian Succession at Site 375

Messinian deposition at this site appears to begin with a period of subaerial exposure and calichefication. The overlying gypsum-bearing deposits were so sparsely cored that interpretation is difficult. The area apparently became submerged to at least shallow depths, and the general pattern of deposition was an alternation of in situ growth of gypsum crystals at the sediment-water interface, and erosion and redeposition of gypsum crystals and other components. Growth of selenite crystals in marl occurred during the latter part of Messinian deposition and the final Messinian event recorded at Site 375 was deposition of nannofossil-bearing dolomitic marl of the "Lago Mare" facies (Ruggieri, 1967). Cores 16 to 20 at Site 376 appear to be contemporaneous with these deposits, and provide a more complete sedimentological record.

#### SITE 376, FLORENCE RISE, WEST OF CYPRUS

Messinian sediments recovered at Site 376 consist of an upper marlstone unit underlain by two evaporitic units. The upper unit, recovered in Cores 7 through 15, comprises mainly dark colored nannofossil-foraminiferal marlstones that are variably dolomitic; interbedded with these are graded turbiditic arenites and siltites. A comprehensive description of this upper unit, representing the "Lago Mare" facies in the sense of Ruggieri (1967), is provided in the Site 376 Report, this volume. It is interpreted as an alternation of hemipelagic sediment and proximal to distal turbidites, forming an overall deepening sequence from bottom to top. Depositional conditions may have resembled those in parts of the Black Sea (Ross and Degens, 1974; Müller and Stoffers, 1974) where fine-grained turbidites are occasionally deposited (Jipa, 1974). Some of the turbiditic layers in the basal part of the unit contain reworked and redeposited clasts of gypsum (cf. Dabrio et al., 1972; Ricci Lucchi, 1973).

The evaporitic rocks at Site 376 consist of an anhydrite-halite sequence overlain by a sequence of gypsum, breccia, arenite, and marlstone. We describe and interpret these two subdivisions below.

### Gypsum Interbedded With Clastic Units and Marlstones

We recovered these lithologies in Cores 16 through 20 between subbottom depths of 140.5 and 188 meters. Except for the last core, continuous coring was attempted in this interval, but recovery was sporadic. In addition, intense drilling disturbance of Cores 16, 17, and 18 reduced most portions of these to drilling breccias consisting of scattered fragments of rocks whose stratigraphic context is commonly uncertain. Our reconstruction of the sediments recovered in these three cores is that they are interbeds of marlstone, clastic arenites, gypsarenites, and gypsrudites plus several other varieties of gypsum, and we interpret them as a transition from in situ growth of gypsum in relatively shallow water (Cores 19 and 20) to deeper water deposition of hemipelagic and turbiditic sediments (Cores 7-15).

Among the varieties of gypsum present, those listed below appear to be the most important.

1) Gypsarenites, typically well cemented, dense and rather well sorted though sometimes containing up to 10% of micritic matrix (Figure 37). These rocks usually are 70% to 90% sand-size gypsum clasts that show diagenetic mosaic intergrowths. Most of the gypsum clasts are clear and monocrystalline, some are twinned, abraded selenite crystals. Impurities present include serpentinite fragments, pyroxene, and what appear to be chloritized basaltic rock fragments. The most abundant nonevaporite constituents are reworked planktonic and benthic foraminiferal tests, and intraclasts and lithoclasts of micritic carbonate.

2) Gypsrudites that appear to have originated as *dissolution breccias* like those present at Site 375. These consist of randomly oriented aggregations of pebble to

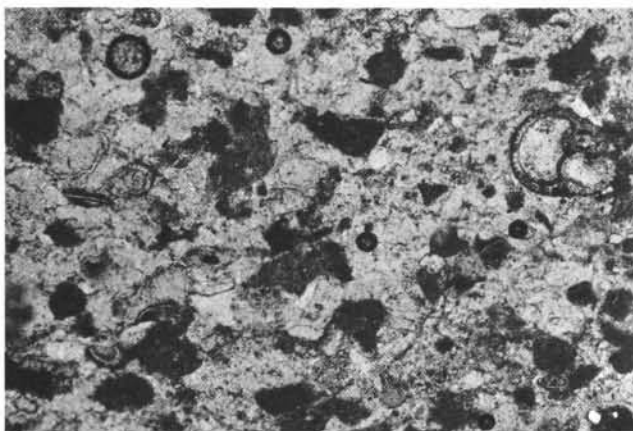


Figure 37. Gypsarenite at Site 376, photomicrograph, plain light. Clastic particles of gypsum (light) mixed with foraminiferal tests and dark lithic fragments. Scale bar is 500  $\mu$ m (376-15-2, 28-29 cm).

sand size, clear gypsum crystals that show tightly interlocking grain boundaries (Figure 38), which in some areas have small amounts of intercrystalline micritic carbonate. Many of the coarse gypsum crystals contain included pellets, probably created by brine shrimp. They also contain patches of micritic carbonate suggesting considerable post-depositional overgrowth has taken place. We interpret these as products of more or less in situ deposition of slightly reworked selenite crystals.

3) Alabastrine gypsum composed of fine-grained, elongated gypsum crystals with felted texture. In hand specimen these rocks are white and dense. They appear to be replacements of felted anhydrite, and coarse mosaic gypsum in turn partly replaces the felted gypsum.

4) Selenitic gypsum consisting of elongate, swallow-tail crystals of gypsum, up to 4 cm and with long axes oriented approximately perpendicular to bedding. These crystals are embedded in a matrix of finer gypsum crystals and greenish white marlstone. The selenite appears to have grown displacively in this marly sediment.

5) Laminated gypsum of several kinds. Some laminated (and cross-laminated) gypsum is fine-

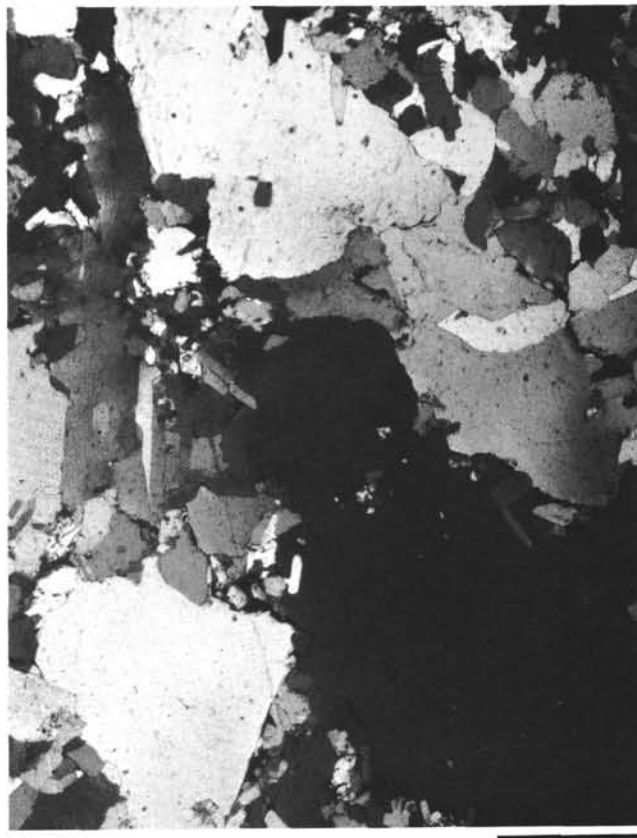


Figure 38. Gypsrudite at Site 376, thin-section photograph, crossed nicols. Poorly sorted mixture of gypsum clasts includes some reworked "swallow-tail" twins at left. Note sutured grain boundaries, the result of diagenetic overgrowths around the clasts. Scale bar is 2 mm (376-18-1, 63-65 cm).

grained gypsarenite that has normal size grading and typically contains abundant elongated gypsum crystals; the latter are very well aligned parallel to bedding, and appear to represent redeposition of gypsum needles precipitated at the air-water interface (see discussion below). Other kinds show well-developed reverse graded bedding similar to that at Site 372. The laminae in these are bounded by thin micritic carbonate micro-laminae, some of which are rich in organic matter and may have been algal stromatolites. Like that at Site 372, the reverse size grading of gypsum clasts was enhanced by early diagenetic recrystallization and crystal growth at the top of individual laminae; in some instances gypsum crystals began to grow up from the sediment-water interface to form thin crusts (Figures 39-41), some of which were reworked by currents or by dissolution (perhaps due to freshening).

Very coarse, secondary gypsum crystals with very irregular boundaries have replaced some laminated gypsum, leaving only the micritic micro-laminae to mark the laminations (Figure 40). Between cross nicols these crystals show a peculiar shimmery appearance at extinction positions, and they appear to have replaced felted masses of small elongated gypsum or anhydrite crystals (cf. Ogniben, 1957).

Rounded aggregations of length-slow chalcedony (lutecite) form small replacement bodies in all of the gypsum, but they are particularly common in the coarse replacement gypsum described in the preceding paragraph.

The range of textures noted above suggests that periods of in situ growth of gypsum crystals on the

bottom alternated with periods of reworking and redeposition of this gypsum. Figure 41 is an example from Core 16 and displays fabrics formed by various of these processes. Coarse selenite crystals grew from the sediment-water interface, but many of these were eroded, possibly due to partial dissolution, and deposited more or less in situ. These processes were succeeded by current or wave deposition of allochthonous gypsum grains to produce the overlying, rather well-sorted, laminated gypsarenite. The depositing current appears also to have slightly eroded the selenitic layer.

Whereas some of the redeposited gypsum layers represent purely local reworking and redeposition, others contain more allochthonous components such as reworked foraminifers, serpentinite fragments, detrital pyroxene, etc. that signify more distant and varied source areas. These are most common near the top of the sequence; and in Section 1 of Core 16, from 36 to 87 cm, they are interlayered with greenish gray marlstone that is similar to the hemipelagic marlstone of the "Lago Mare" facies that occur stratigraphically above in Cores 15 through 7.

Cores 19 and 20 are much less disturbed by coring than Cores 16, 17, and 18. Core 19 contains about 30 cm of poorly sorted gypsrudite with angular to subrounded clasts, up to 5 cm in maximum dimension (Figures 42 and 43). Fabric varies from tightly packed clasts to clasts which are embedded in sparse, pale green sandy marlstone. The most abundant clasts are large, single gypsum crystals most of which look like redeposited selenite; some of these clasts have secondary overgrowths that give them a euhedral form. The second most abundant and the largest clasts are lami-

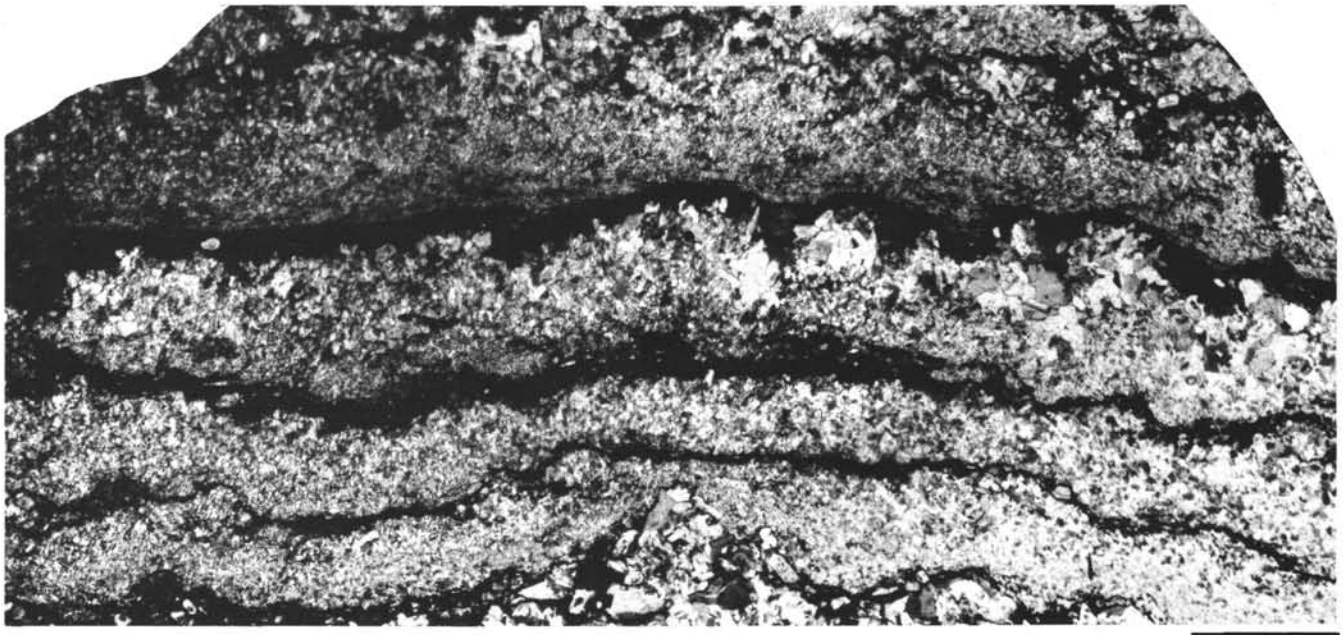


Figure 39. Laminated gypsum at Site 376, thin-section photograph, partly crossed nicols. Note reverse grading in laminae produced by diagenetic growth of coarse crystals at tops of laminae. Many of these crystals show elongation perpendicular to bedding. Dark micro-laminae between gypsum laminae are organic-rich micritic carbonate, and were probably algal stromatolites. Scale bar is 2 mm (376-16-1, 140-145 cm).

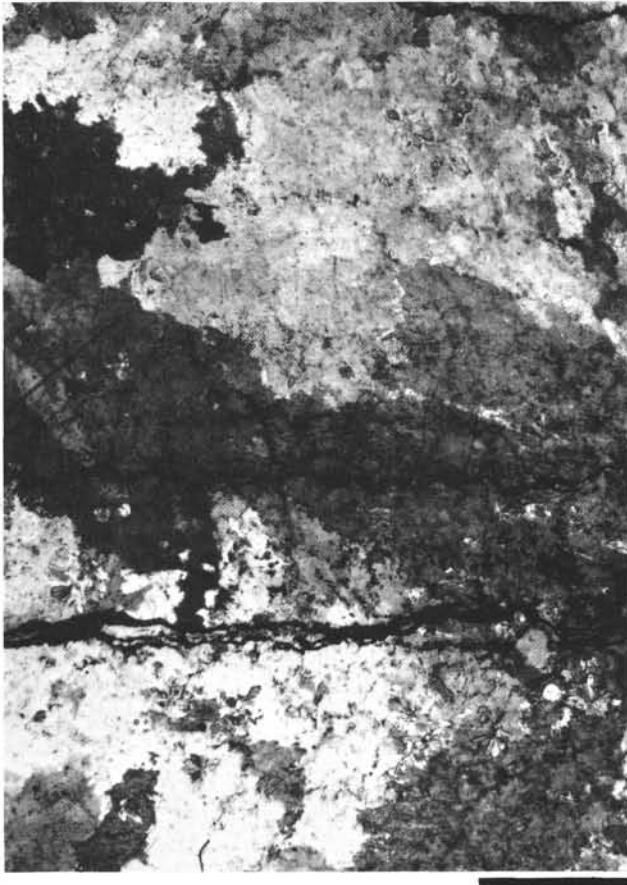


Figure 40. *Laminated gypsum at Site 376, thin-section photograph, partly crossed nicols. Recrystallization has produced a coarse mosaic of gypsum crystals with very irregular crystal boundaries. Micritic micro-laminae, rich in organic material, like that in bottom center and top right, bound the larger scale laminations. Scale bar is 2 mm (376-16-1, 18-22 cm).*

nated gypsarenites, typically present as elongated fragments. Other grains are several varieties of fine-grained limestone including laminated and algal limestone with bird's eye (fenestral) structure, large benthic foraminifers, altered planktonic foraminifers (some cemented in micritic carbonate), pelecypod shell fragments, fine-grained dolomite, and various silicate grains including green hornblende, altered (chloritized) volcanic rock fragments, and a little quartz. These are cemented in variable amounts of micritic carbonate, and secondary overgrowth on coarser gypsum crystals has been relatively minor in cementing this rock.

The bottom 10 cm of Core 19 and all of Core 20 consists of generally well sorted, olive-gray to black gypsiltites, gypsarenites, and fine gypsrudites with small amounts of micritic matrix. Many of these are very finely laminated, and some contain thin, wavy dark micro-laminae which are rich in organic material and resemble algal stromatolites. Some of the laminated gypsum shows small-scale deformation and microfaulting, possibly a result of compactional or dewatering stresses. In comparison with the overlying

gypsum-bearing clastic rocks, these are relatively pure gypsum rocks with smaller amounts of reworked foraminifers and carbonate rocks, and with only some silicate clasts.

Much of the detrital gypsum forms a recrystallization mosaic, except where sufficient intergranular micritic matrix apparently inhibited secondary overgrowths (Figure 44). The coarser layers contain numerous lozenge-shaped gypsum crystals that appear to be reworked selenite with secondary overgrowths (Figure 45C). A common texture in unrecrystallized gypsarenites is highly oriented gypsum needles with elongate dimension, parallel to stratification (Figure 45B). This crystal form, common also in the overlying gypsarenites, is produced by gypsum crystallization within water, either at the air-water interface or at the sediment-water interface (Kinsman, 1969; Edinger, 1973), from which it was apparently concentrated by currents and deposited in laminae. A similar gypsarenite from the Miocene of Cyprus is shown in Figure 45A.

#### Anhydrite and Halite of Cores 22 and 23

Core 21 had no recovery and probably penetrated halite that dissolved during coring. Cores 22 and 23 recovered about 140 cm of interlayered halite and anhydrite, similar to that cored in the Red Sea at Sites 225 and 227 (Stoffers and Kuehn, 1974). The upper 50 cm of Section 1, Core 22 comprise mainly broken pieces of banded halite. In the latter, millimeter-thick, wavy laminae of gypsum separate beds, 1 to 5 cm thick, of translucent halite. The halite is mainly in the form of coarse crystals that appear to be products of recrystallization (Figure 45D). Some crystals contain inclusion-outlined traces of former crystals, but we recognized no distinctive primary features like chevron structure. The bottom 15 cm of Section 1, Core 22 consist of similar banded halite. The relatively low bromine content of this halite suggests some reworking in fresh water (Kuehn and Hsü, this volume), which could account for the apparent high degree of recrystallization.

Between the two halite intervals noted above is about 50 cm of nodular to laminated white anhydrite. This interval contains several enterolithic folds (Figure 46) along with well developed nodular or chicken-wire structure (the latter between 100 and 106 cm). The bottom 6 cm of the anhydrite are irregularly laminated. They contain laminae, 0.5 to 1.0 cm thick, of coalesced nodules; dark brown micro-laminae separate the layers. Throughout the anhydrite are small irregularly shaped patches of clear halite; some of these, especially in the laminated anhydrite, resemble fenestral voids filled secondarily by halite.

This anhydrite comprises the typical felted mass of laths with long dimensions that are largely between 50 and 300  $\mu\text{m}$  long. There is, however, considerable replacement by coarse secondary gypsum, and in some places large poikilitic gypsum crystals engulf anhydrite laths. Squeezed between nodular anhydrite bodies are thin seams of dark brown, organic matter-rich, fine-grained dolomite.



Figure 41. *Laminated gypsum at Site 376, thin-section photograph, partly crossed nicols. In the lower half, a few vertically oriented, twinned selenite crystals are bordered by a poorly sorted rubble of clastic gypsum grains. Overlying this coarse layer is micro-laminated, fine-grained clastic gypsum and micrite which includes a few large gypsum clasts like that at the top. We interpret this fabric as an alternation of in situ growth of selenite and reworking and redeposition of gypsum by currents. Scale bar is 2 mm (376-16-1, 124-129 cm).*

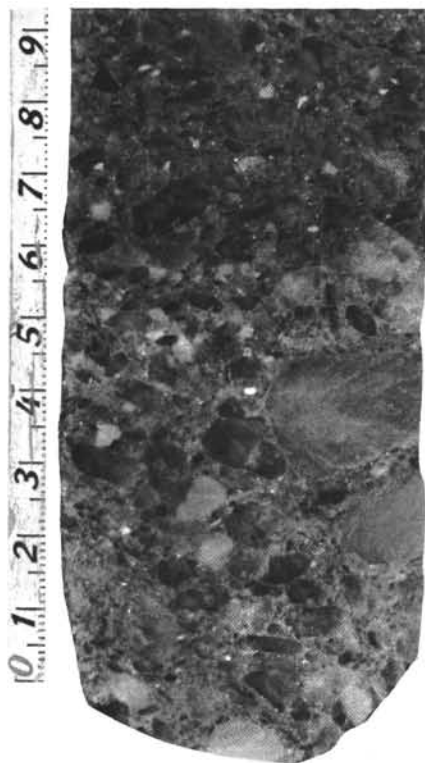


Figure 42. *Gypsrudite at Site 376, core photograph. Rounded to angular pieces of clastic gypsum rest in a matrix of marlstone and fine-grained clastic gypsum. Scale is in centimeters (376-19-1, 115-125 cm).*

Core 23 is a drilling breccia and consists of about 30 cm of rubble of small, broken pieces of layered anhydrite and translucent halite. These appear identical to the halite and anhydrite in Core 22.

#### Interpretation of Messinian Evaporites at Site 376

As at Site 374, the vertical succession of facies at Site 376 records a progressive decrease in salinity; it probably records, as well, a progressive deepening of water.

The anhydrite at the base of the cored section (Cores 22 and 23) contains a variety of textures and structures identical to those in anhydritic sediments of Persian Gulf sabkhas; among these are enterolithic folds, chicken-wire structure, irregular laminations, and possible fenestral structures. Dean et al. (1975) have prescribed caution in restricting the interpretation of these structures to the sabkha environment, pointing out that diagenesis produces all of them. They argue, for example, that deep water, laminated anhydrites can alter into highly nodular and enterolithically folded anhydrites. However, no vestiges of evenly laminated anhydrite of the kind they describe remain at Site 376; thus, if the anhydrite there were originally evenly laminated and deposited in deep water, one would have to assume total transformation to a highly nodular enterolithically folded rock. We believe, how-

ever, the sabkha interpretation accounts much better for the character of this anhydrite and for its association with shallow water gypsum deposits that lie above it.

We found no independent evidence regarding the environment and water depth in which the halite was deposited, as diagenetic recrystallization appears to have destroyed most primary fabrics in this rock. However, because of its close stratigraphic association with the anhydrite, we assume that the halite too was deposited in a shallow water or intermittently flooded environment, perhaps one somewhat similar to Salina Ometepec in Baja California where banded halite-gypsum rock forms today (Shearman, 1970). The low Bromine content of the halite and the low strontium content of the thin gypsum layers in it suggests that continental waters diluted the brines (Kuehn and Hsü, this volume), which would be compatible with formation in a subaerially exposed evaporite flat.

Above these saline phases is a facies dominated by gypsum deposition (Cores 16-20). But, instead of

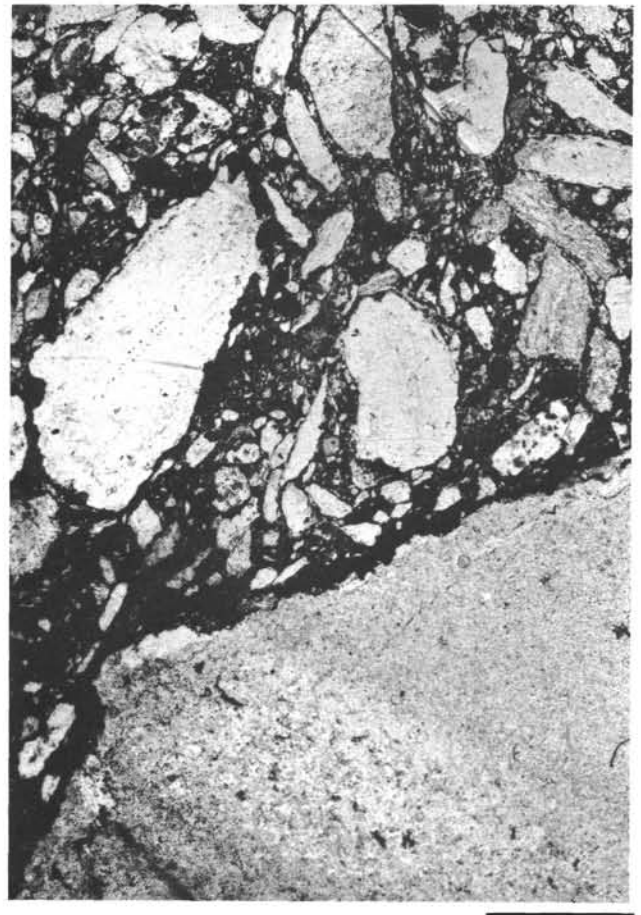


Figure 43. *Gypsrudite at Site 376, thin-section photograph, plain light. Poorly sorted assemblage of angular gypsum clasts in dark micritic matrix. The clasts of gypsum include laminated gypsum (large clast at lower right) as well as coarse monocrystalline fragments. Scale bar is 2 mm (376-19-1, 129-133 cm).*

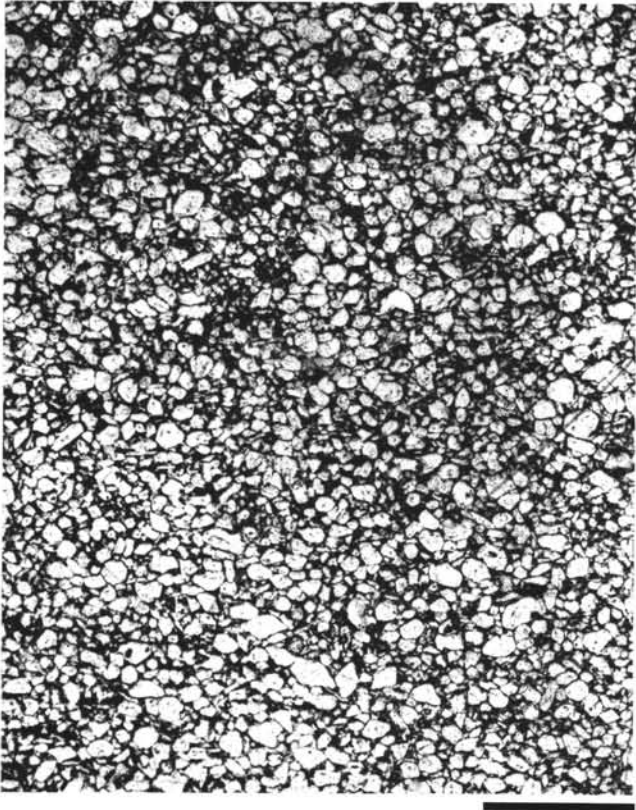


Figure 44. Gypsarenite at Site 376, thin-section photograph, plain light. Well sorted, sand-size clasts of monocrystalline gypsum, with sparse micrite matrix (dark). Scale bar is 2 mm (376-20-1, 122 cm).

gypsum-mudstone cycles like those at Site 374, the pattern of deposition was much like that at Site 375. Periods of in situ precipitation of gypsum, commonly as selenite crystals growing on the bottom, alternated with periods during which this gypsum was eroded, reworked, and redeposited, sometimes with admixtures of allochthonous micro-fossils, carbonate lithoclasts, and detrital silicate components. We believe all of these processes occurred in a relatively shallow water environment, periodically affected by high energy events such as storms.

We interpret the stratigraphically highest Messinian unit, the hemipelagic marlstones and the graded, clastic turbidite beds of Cores 7 through 15, as signifying deeper and less saline water of the "Lago Mare" stage (see discussion in Site 377 report, this volume).

#### SITE 378, NORTH CRETAN BASIN

Messinian sediments recovered from the two holes drilled at this site consist of: (1) a small amount of dolomitic caliche breccia, and (2) several meters of coarse selenitic gypsum.

##### Dolomitic Caliche Breccia

The core-catcher sample of Core 11, Hole 378 contained two pieces of this breccia which we surmise occurred near the contact between Pliocene nannofossil

marlstone and the underlying selenitic gypsum (see discussion in Site 378 report, this volume). The major mineral present is calcium-rich dolomite with approximately 5 mol % excess  $\text{CaCO}_3$ . The rock consists of subrounded carbonate lithoclasts, up to 1 cm across, cemented in a matrix of dolomicrite and microspar that is very porous and contains irregularly shaped vugs up to one-half millimeter long (Figure 47). The microspar becomes somewhat coarser toward the edges of the vugs, and microspar crystals that line the vugs show rough orientation as if they were void fillings.

Most of the clasts are very fine-grained dolomite in which all traces of primary texture seem to have been destroyed; a few clasts, however, have ghost-like outlines of altered micro-fossils, possibly foraminifers. Commonly the edges of the clasts are indistinct. Some clasts are medium-grained sparite, and these have fine-grained dolomitic coatings, typically 0.5 mm thick.

Among the alteration processes which have affected this rock are fragmentation, micritization, recrystallization, dolomitization, solution, and cementation. James (1972) has shown that this range of alteration processes, with the exception of dolomitization, can result from subaerial exposure of carbonate rocks. Walls et al. (1975) emphasized the brecciation of carbonate rocks during subaerial exposure and calichefication. Scholle and Kinsman (1974) described formation of caliche in vadose environments near the Persian Gulf where vadose and phreatic pore waters have very high salinities and high concentrations of magnesium. As a result the caliche crusts which formed there consist of aragonite and high magnesium calcite, and small amounts of dolomite. The latter, in the view of Scholle and Kinsman, may signify the beginning of penecontemporaneous dolomitization, leading eventually to complete dolomitization.

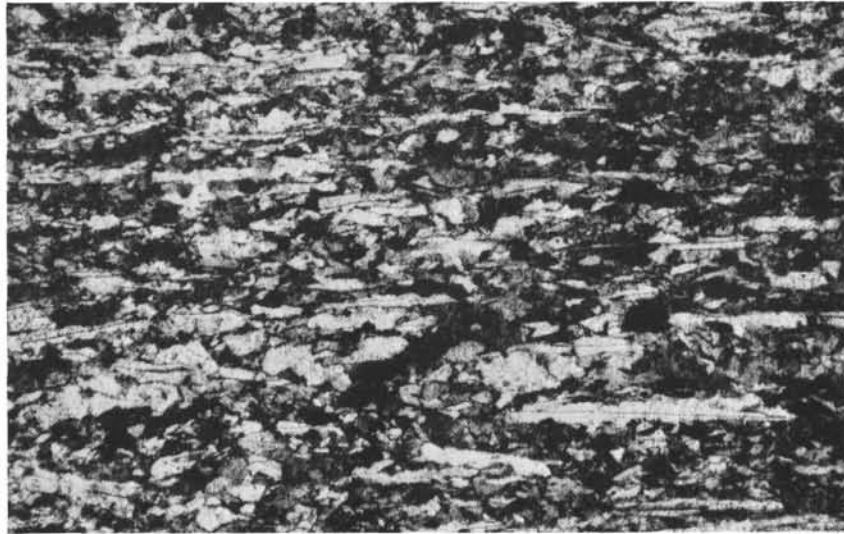
We interpret this rock as a calichified and dolomitized carbonate breccia formed subaerially in a setting somewhat like that described by Scholle and Kinsman (1974), i.e., an area characterized by highly saline pore waters. The stable isotope values of this rock are:

$$\delta\text{O}_{\text{PDB}}^{18} = +4.2, \delta\text{C}_{\text{PDB}}^{13} = +2.3$$

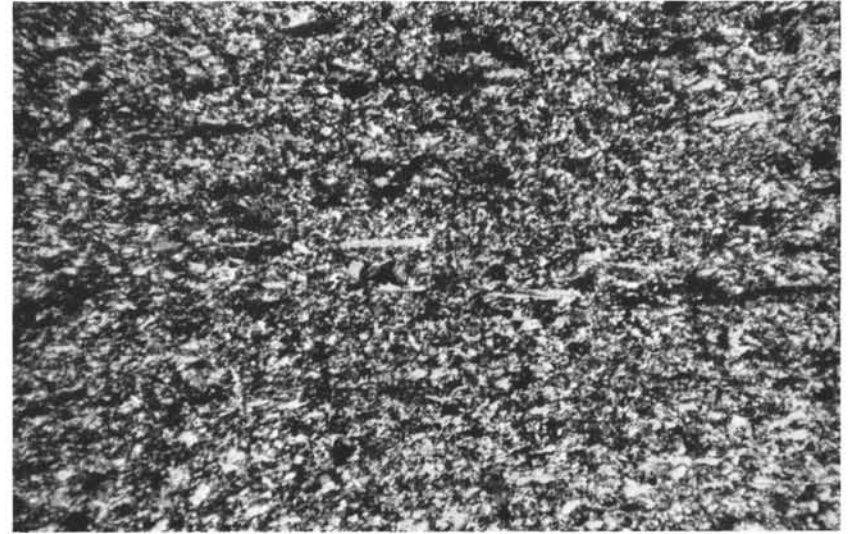
These values would be normal for a calcium-rich dolomitic precipitated interstitially from evaporated waters, as with the Recent dolomite from Abu Dhabi sabkhas (J. McKenzie, personal communication, 1976). Somewhat similar, subaerially altered carbonate rocks occur in the Messinian "Calcare di base" of Sicily. Ogniben (1963) attributes the vugginess and breccia texture of some rocks in the Calcare di base to dissolution of halite.

##### Coarse Selenitic Gypsum

Cores 4, 5, and 6 at Site 378A are selenitic gypsum recovered from subbottom depths of 302 and 331 meters. Because both coring and recovery were not continuous in that interval, we are uncertain whether



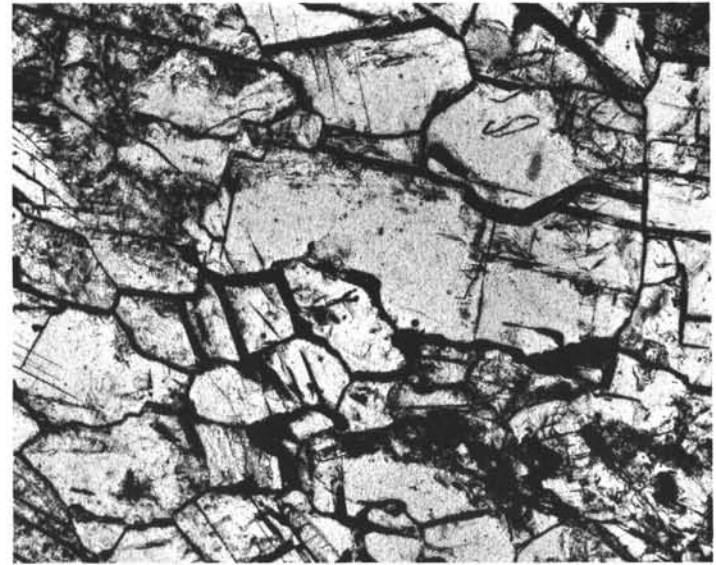
A



B



C



D

Figure 45. Photomicrographs of Miocene evaporites from Cyprus and at Site 376. Photos A, B, and C are with partly crossed nicols, D with plain light. Scale bars are 500  $\mu\text{m}$ . (A) Laminated gypsum from the Lapatkos Formation, upper Miocene, Cyprus. This rock consists of elongated gypsum crystals, apparently reworked and redeposited by currents. Note that many of these crystals are twinned and have irregular grain boundaries due to diagenetic overgrowths. (B) Laminated gypsum from Site 376, somewhat like A, but finer grained and containing fewer elongated gypsum crystals (376-20-1, 71-74 cm). (C) Laminated gypsum from Site 376. The laminae in this sample consist of alternations of coarse and fine-grained gypsum (cf. Figure 36). This photograph is of a coarse layer which consists of small selenite crystals some of which appear to have been slightly reworked; these now lie with their long axes more or less parallel to bedding, instead of in the upright position characteristic of in situ growth. Some of these selenite crystals have secondary overgrowths, which give them a doubly terminated appearance (376-20-1, 61-64 cm). (D) Halite from Site 376. A coarse-grained recrystallization mosaic of halite crystals containing inclusions of micrite and other impurities.

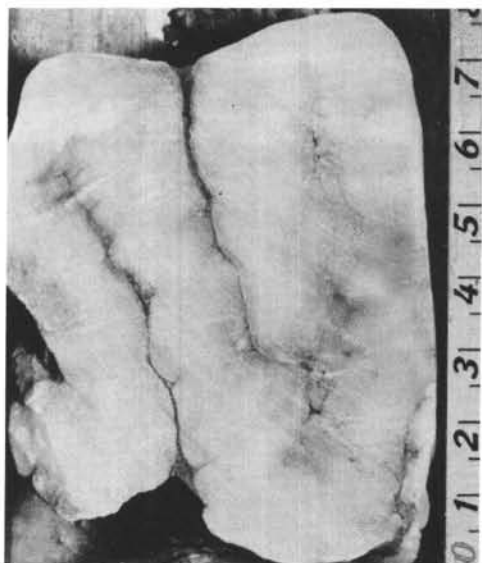


Figure 46. Enterolithic fold in nodular anhydrite, Site 376, core photograph. Scale at right is in centimeters (376-22-1, 85-93 cm).

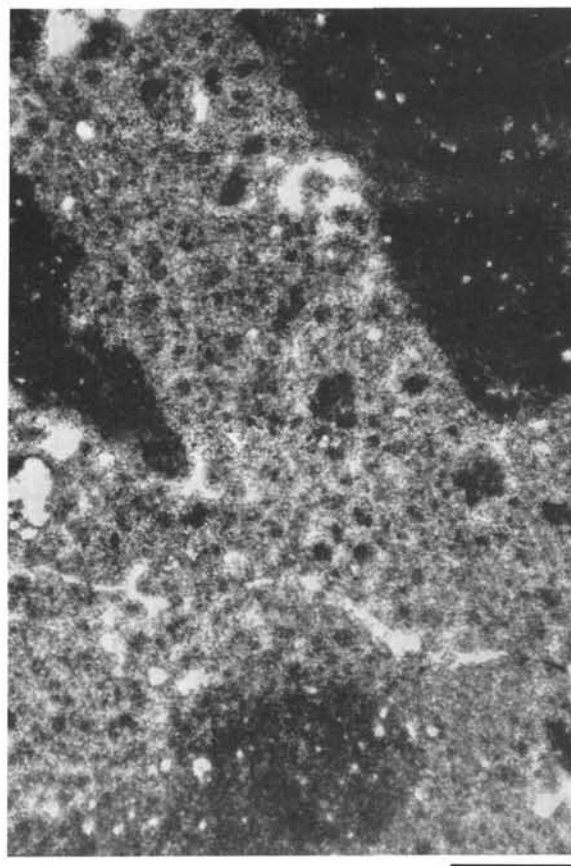


Figure 47. Dolomitic caliche breccia, Site 378, photomicrograph, plain light. Dark angular clasts of fine-grained dolomite are apparently remnants of an intensively altered limestone. These clasts are cemented in a porous matrix of peloidal fine-grained dolomite. Scale bar is 500  $\mu\text{m}$  (378-11, CC).

the entire interval is selenite or whether the selenite occurs as several layers separated by other lithologies.

The selenite crystals are elongated and commonly twinned ("swallow-tail" structure), and single crystals are up to 8 cm in length (cf. Ogniben, 1954; Richter-Bernburg, 1973). In parts of these cores, particularly the bottom part of Core 5, the long axes of these crystals are oriented perpendicularly to bedding or at high angles to it. Commonly, these crystals are euhedral and aggregated in clusters that seem to radiate upward and outward from a single area of a substrate.

Most of the selenitic crystals, however, lack this perfection of orientation. Although many of them are still elongated at high angles to bedding, they are surrounded by aggregations of crystals that are more randomly oriented. In addition, the individual crystals are typically less well formed compared to those in the spherulitic clusters; they have an etched appearance, and typically form interlocking mosaics with adjacent crystals. We believe this kind of fabric results from growth-dissolution cycles of the kind seen in Messinian selenitic gypsum on Sicily (Schreiber, 1974) and discussed in a following section.

Some parts of the cores retain primary intercrystalline porosity. More commonly, however, these are relatively nonporous rocks. In some instances, micritic carbonate or fine-grained gypsum fills the intercrystalline areas, in others secondary gypsum overgrowths have acted to fill these voids, producing irregular, tightly interlocking crystal boundaries (Figure 48). Thin stringers of micritic carbonate remain to outline the original crystal boundaries in a few cases.

Some crystals contain a few small laths of euhedral anhydrite which they seem to have poikilitically included, perhaps during secondary overgrowth. More common forms of inclusions within selenite are small

spherical eggs and ovoid micritic pellets (Figure 48), both probably the products of brine shrimp or similar animals. The former are circular bodies of organic material up to 250  $\mu\text{m}$  in diameter. The pellets are typically ovoid, micritic, and are usually less than 150  $\mu\text{m}$  in maximum dimension.

As noted in our discussion of Site 376, selenitic gypsum of this kind has been described in Miocene and Pleistocene deposits of Sicily, as well as in a number of modern environments. In recent years, most workers who have studied the Sicilian selenites interpret them as primary and mostly of shallow water origin. This interpretation is supported by a limited number of observations in modern artificial salt ponds and hypersaline natural environments (cf. Goto, 1967; Hardie and Eugster, 1971; Schreiber and Kinsman, 1975; Vonder Haar and Gorsline, in press).

By analogy with modern and most ancient occurrences, we are left with the impression that the selenitic gypsum at Site 378 formed in very shallow water, but there is no independent evidence for this, such as algal stromatolites. The presence of probable fecal pellets and eggs of brine shrimp, and the association with

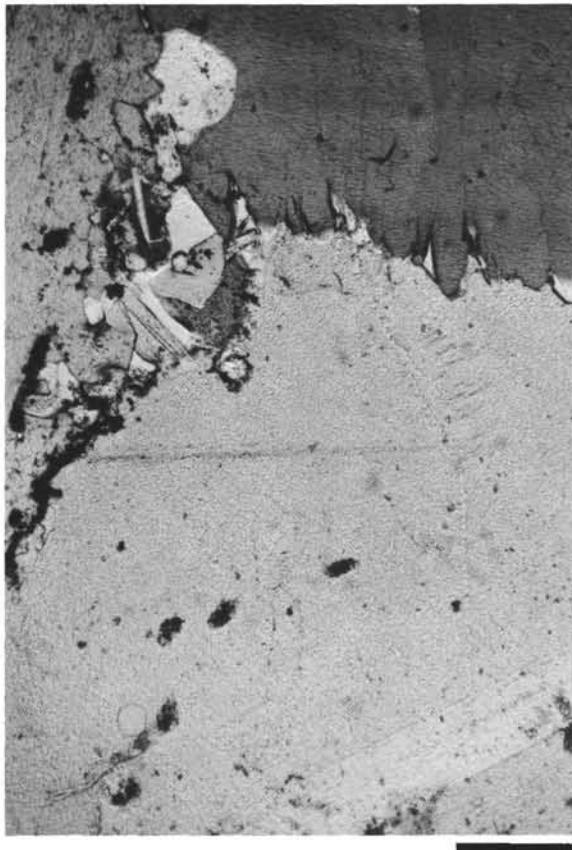


Figure 48. *Selenitic gypsum, Site 378A, photomicrograph, partly crossed nicols. Note sutured intercrystalline boundaries, probably the result of diagenetic overgrowth. Small, dark oval bodies are fecal pellets, possibly of brine shrimp. Scale bar is 500  $\mu$ m (378A-4-1, 40-43 cm).*



Figure 49. *Selenite from Gessoso-Solfijera Formation, upper Miocene, Eraclea Minoa, Sicily. Regular beds of radiating gypsum crystals elongated perpendicularly or nearly so to stratification. Specimen is about 20 cm high.*

caliche breccia, however, act to strengthen the shallow water interpretation.

#### SELENITE DISSOLUTION BRECCIAS

Comparison with the Sicilian selenitic layers (Figures 49-51) yields insights regarding the diagenetic history of the selenite at Sites 378, 375, and 376. Precipitation of primary gypsum under subaqueous conditions results in nucleation of separate crystals, clusters or beds of crystals, followed by slow incremental growth (see Goto, 1967; Orti Cabo and Shearman, in press). Slight phases of undersaturation (refreshment) may cause dissolution of some of the precipitate, but unless the refreshment becomes severe, renewed concentration gives rise to continued precipitation on the original crystal surfaces (Schrieber and Kinsman, 1975). If the continuity of precipitation is sufficiently interrupted, renewed concentration may initiate a new phase of nucleation resulting in a new row of crystals not in continuity with the underlying layer (Figure 49). This interruption may be marked by accumulation of carbonate residue as well as by simple dissolution.

If the interruptive phase of refreshment within the water body results in prolonged exposure of the pre-

existing gypsum to undersaturated waters, then considerable dissolution may result. In the initial phases of refreshment, the affected crystals remain in much the same order as that of formation, exhibiting only dissolution of their terminal faces. Lateral dissolution along the crystal sides may then also become evident, causing these crystals to appear to be less well formed than previously (Figure 50). They may then become etched along adjoining lateral surfaces, and residual accumulations of impurities may collect along these etched boundaries. Renewed precipitation results in crystal overgrowths within dissolution voids and an interlocking mosaic structure is developed. Renewed precipitation also results in the formation of a new layer of crystals along the upper surface along the affected gypsum. Repeated cycles of this sort are common in Cores 4, 5, and 6 of Site 378.

In the final and most extreme stage of dissolution, many of the crystals lose their semiperpendicular orientation such that they are no longer in their growth position and form a residual breccia of the kinds found at Sites 375 and 376. Not all zones of a section are equally affected, as may be seen in Figure 51. The zone indicated as (A) still retains crystal orientation; (B) reflects extensive dissolution, while (C) is a row of

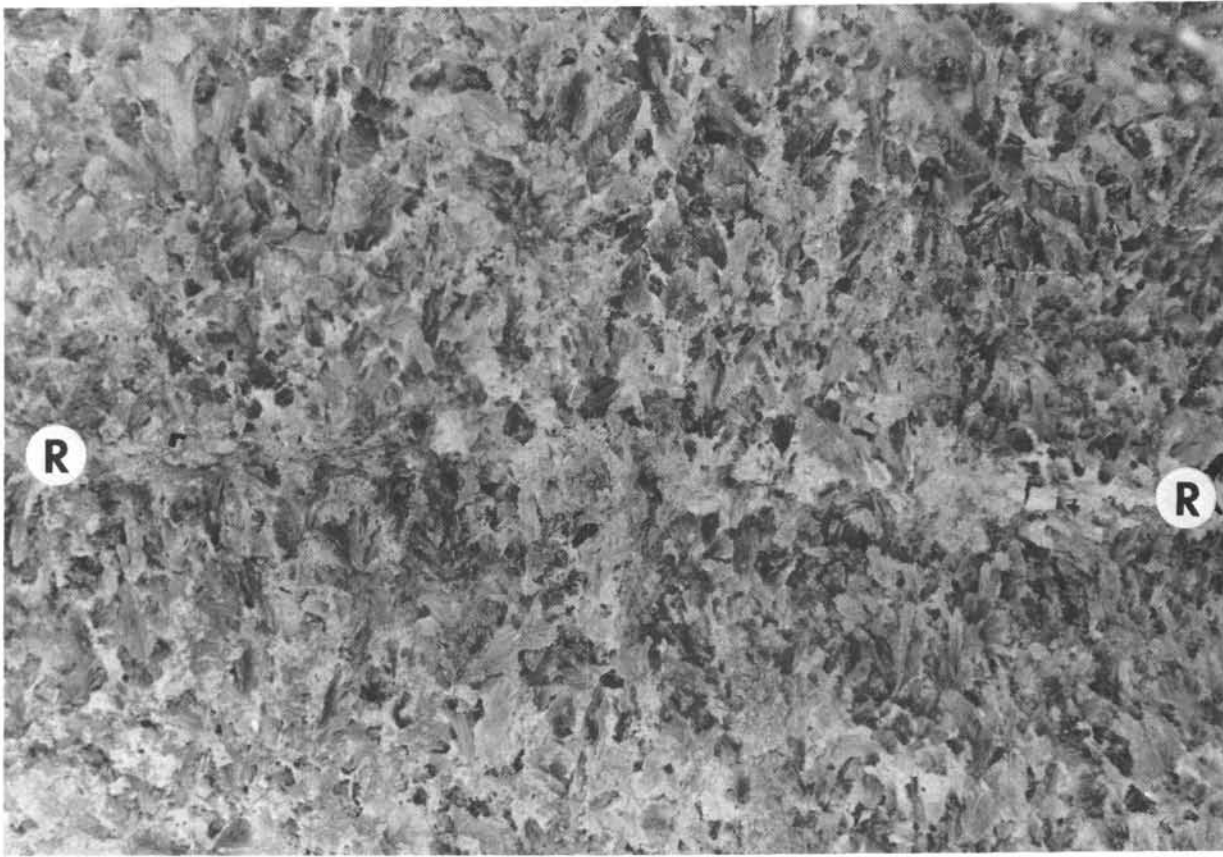


Figure 50. *Selenite from Gessoso-Solfifera Formation, upper Miocene, M. Grotticelli, Sicily. This bed of gypsum shows a number of growth cycles modified by partial dissolution and undermining of the elongated selenite crystals; most of the selenite crystals, however, are very nearly in their original vertical growth positions. The letters "R" mark the ends of a residual layer in which dissolution was more intense. Scale bar is 1 cm. Selenite at Sites 375 and 378A show similar fabrics.*

newer crystals, formed after the events shaping (A) and (B). The terminal ends of this row of crystals are also damaged (see arrows). Long sequences of this kind are noted not only in the Leg 42A cores but also from extensive deposits in the Messinian of Sicily and the Apennines.

#### LAMINATED GYPSUM

Laminated gypsum occurs at Sites 372, 374, 375, and 376, and we wish here to call attention to the presence of several varieties. Most of the laminated gypsum we encountered appears to consist of current-deposited alternations of micrite and/or argillaceous material and clastic gypsum particles, either in inversely graded laminae (Figures 8, 15, and 39) or normally graded laminae (Figure 35). Some of the particles are highly acicular crystals (Figure 45B) and may represent suspension settling rather than current deposition. Several post depositional processes acted to modify this basic pattern. One was the probable growth of algal mats on tops of laminae (Figures 9 and 39). Another process was neomorphic growth of gypsum during early diagenesis, as secondary overgrowths around the clastic gypsum particles and as small selenite crystals growing vertically from the tops of laminae (Figures 7, 8, 10, 36, 39, 41, and 45C). In

some instances, succeeding currents eroded and reworked these crystals (Figure 41). A third modifying process was pervasive recrystallization of the gypsum, perhaps during burial diagenesis, to a relatively coarse mosaic of irregular gypsum crystals that cut across all earlier elements of fabric (Figures 24, 26, 27, and 40).

#### SUMMARY

Table 1 summarizes the main features of Messinian sediments cored during Leg 42A and lists the inferred depositional environments, along with a few comparable modern and ancient environments. The latter listings are not comprehensive. The ancient examples, for example, purposely emphasize on-land Messinian evaporite successions from the circum-Mediterranean region; and both the ancient and modern examples are not meant to be perfect analogs, but only illustrations which share some common characteristics with the Messinian sediments from Leg 42A. Extensive research now in progress on evaporite sedimentology should result in refinements of our interpretations within the next few years. We feel, however, that our overall assessment of most of these sediments as shallow water to subaerial deposits will be verified by future investigations.

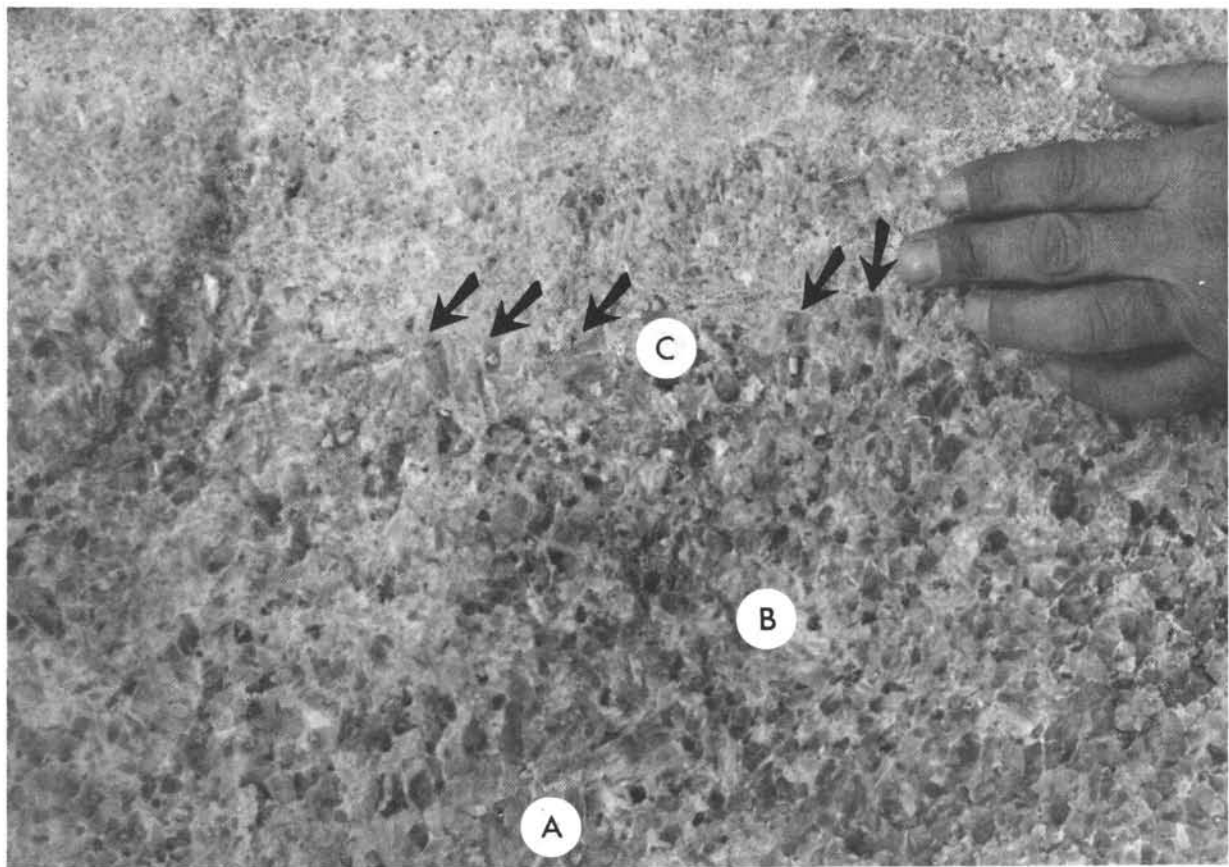


Figure 51. *Outcrop of selenite in Gessoso-Solfifera Formation, upper Miocene, M. Grotticelli, Sicily. This outcrop shows the transition to a gypsum dissolution breccia. The zone marked A is relatively unaffected and still shows vertical crystal orientation. Zone B is a rubble of resedimented selenite crystals, a dissolution breccia, similar to rocks recovered at Sites 375 and 376 (cf. Figure 38). Zone C is a bed of later crystal growth; the crystals retain their upright positions, but solution has blunted the crystal tips (indicated by arrows).*

#### ACKNOWLEDGMENTS

We are grateful to Stephen Vonder Haar and Franco Ricci Lucci for reviewing the manuscript and for helpful discussions and suggestions; to Eugenio Gonzales and L. Horan for technical help; to Judy McKenzie for supplying us with a light isotope analysis; and to D. G. Moore for support in making this collaborative effort possible. A grant from the Faculty Research Committee of the University of California, Santa Cruz, helped to defray costs of sample preparation.

#### REFERENCES

- Arthurton, R. S., 1973. Experimentally produced halite compared with Triassic layered halite-rock from Cheshire, England: *Sedimentology*, v. 20, p. 145-160.
- Bandy, O. O., Butler, E. A., and Wright, R. C., 1969. Alaskan Upper Miocene marine glacial deposits and the *Turborotalia pachyderma* datum plane: *Science*, v. 166, p. 607-609.
- Bebout, D. G. and Maiklem, W. R., 1973. Ancient anhydrite facies and environments, Middle Devonian Elk Point Basin, Alberta: *Canadian Petrol. Geol. Bull.*, v. 21, p. 287-293.
- Bertrand, J. P. and Jelisejeff, A., 1974. Formation d'évaporites par des processus d'évaporation capillaire: *Rev. Géogr. Phys. Géol. Dynamique*, v. 16, p. 161-170.
- Braune, K., Fabricius, F., and Heimann, K. O., 1973. Sedimentation and facies of Late Miocene strata on Cephalonia (Ionian Islands, Greece). *In* Drooger, C. W. (Ed.), *Messinian Events in the Mediterranean: Geodynamics Sci. Rept No. 7*, p. 192-201.
- Bosellini, A. and Hardie, L. A., 1973. Depositional theme of a marginal marine environment: *Sedimentology*, v. 20, p. 5-17.
- Butler, G. P., 1970. Holocene gypsum and anhydrite of the Abu Dhabi Sabkha, Trucial Coast: an alternative explanation of origin. *In* Rau, J. L. and Dellwig, L. F. (Eds.), *Third Symp. on salt*. Northern Ohio Geol. Soc., p. 120-152.
- Clifton, H. E., 1969. Beach lamination: nature and origin: *Marine Geol.*, v. 7, p. 553-559.
- Dabrio, C. J., Garcia-Yebra, R., Gonzalez-Donoso, J. M., and Vera, J. A., 1972. Turbiditas asociadas a evaporitas (Mioceno, La Mala, depresion de Granada): *Cuad. Geol., Univ. de Granada*, p. 139-164.
- Dean, W. E., Davies, G. R., and Anderson, R. Y., 1975. Sedimentological significance of nodular and laminated anhydrite: *Geology*, v. 3, p. 367-372.

TABLE 1  
 Summary of Characteristics and Depositional Environments for Messinian Sediments, Leg 42A

Cores	Main Characteristics	Inferred Depositional Environments	Some Comparable Modern Environments	Some Comparable Ancient Examples
<b>Site 371</b> 8	Nodular and banded anhydrite overlying barren dolomitic mudstone	Sabkha	Trucial Coast (Kinsman, 1966; Butler, 1970)	Numerous examples cited in Shearman (1971)
<b>Site 372</b> 4-7	Marls and laminated to nodular gypsum	Sabkha to hypersaline lagoon (?)	Trucial Coast (as above)	Upper Miocene, Tunisia, (Bertrand and Jelisejeff, 1974; Shearman, 1971).
8	Laminated gypsum	Evaporite flat or hypersaline lagoon	Laguna Mormona, Mexico (Vonder Haar, 1976)	Upper Miocene, Sicily (Hardie and Eugster, 1971)
9	Laminated marls	Hypersaline lagoon or stagnant basin (?)	Black Sea? (Ross et al., in press)	—
<b>Site 374</b> 12-15	Dolomitic mud and mudstone	Subaqueous (Lago Mare)	Black Sea (Ross and Degens, 1974; Müller and Stoffers, 1974)	Plio.-Quaternary Black Sea (Ross et al., in press)
16-20	Gypsum-mudstone cycles	Shallow subaqueous to subaerially exposed evaporite flat	Laguna Mormona, Mexico (Vonder Haar, 1966); Laguna Madre, U.S.A. (Masson, 1955); Sabkha el Melah de Zarsis, Tunisia (Perthuisat, 1974, 1975)	Upper Miocene, Sicily (Ogniben, 1957; Richter-Bernburg, 1973; Heimann and Masclé, 1974); upper Miocene, Tunisia (Bertrand and Jelisejeff, 1974)
21-22	Nodular anhydrite and halite with minor bittern salts	Sabkha and evaporite flat	Salina Ometepec, Mexico (Thompson, 1968; Shearman, 1970); Laguna Ojo Liebre, Mexico (Phleger, 1969; Holser, 1966); Trucial Coast (Kinsman, 1966, 1969; Butler, 1970)	Upper Miocene, Red Sea (Stoffers and Kühn, 1974); Triassic, England (Arthurton, 1973); Sabkha examples cited in Shearman (1971)
<b>Site 375</b> 1-3	Gypsum (selenitic, laminated, coarse clastic) and dolomitic caliche breccia	Shallow subaqueous to subaerial	See Site 374, Cores 16-20	See Site 374, Cores 16-20
<b>Site 376</b> 7-15	Marlstone with interlayered turbidites	Subaqueous (Lago Mare)	Black Sea? (Ross and Degens, 1974; Müller and Stoffers, 1974; Jipa, 1974)	Upper Miocene, Italy (Ricci Lucchi, 1973; Schreiber et al., 1976). Plio. Quat. Black Sea (Ross et al., in press)
16-20	Gypsum (clastic, selenitic laminated)	Shallow subaqueous; possibly at times a subaerially exposed evaporite flat	See Site 374, Cores 16-20	See Site 374, Cores 16-20
22-23	Nodular anhydrite and halite	Sabkha and evaporite flat	See Site 374, Cores 21-22	See Site 374, Cores 21-22
<b>Hole 378</b> 11, CC	Dolomitic caliche breccia	Subaerial exposure of carbonate rock	James (1972); Scholle and Kinsman (1974)	Upper Miocene, Sicily (Schreiber, 1974; Carboniferous, USA (Walls et al., 1975)
<b>Hole 378A</b> 4-6	Coarse selenite	Shallow subaqueous	Australia (Goto, 1967); S. F. Bay, U.S.A. (Schreiber and Kinsman, 1975)	Pleistocene, Sicily (Schreiber and Kinsman, 1975); Upper Miocene, Sicily (Ogniben, 1957; Hardie and Eugster, 1971; Richter-Bernburg, 1973; Schreiber et al., 1976, in press. U. Miocene, Spain (Orti Cabo and Shearman, in press)

Decima, A. and Wezel, F. C., 1971. Osservazioni sulle evaporiti messiniane delle Sicilia centro-meridionale: *Rev. Mineraria Siciliana*, v. 22, p. 172-187.

———, 1973. Late Miocene evaporites of the central Sicilian Basin, Italy. *In* Ryan, W. B. F., Hsü, K. J., et al., Initial Reports of the Deep Sea Drilling Project, Volume 13; Washington (U. S. Government Printing Office), p. 1234-1239.

Edinger, S. E., 1973. The growth of gypsum: *J. Crystal Growth*, v. 18, p. 217-224.

Folk, R. L. and Pittman, J. S., 1971. Length-slow chalcedony: a new testam for vanished evaporites: *J. Sediment. Petrol.*, v. 41, p. 1045-1058.

Friedman, G. M., 1973. Petrographic data and comments on the depositional environment of the Miocene sulfates and dolomites at Sites 124, 132, and 134, western Mediterra-

nean Sea. *In* Ryan, W. B. F., Hsü, K. J., et al., Initial Reports of the Deep Sea Drilling Project, Volume 13: Washington (U. S. Government Printing Office), p. 695-708.

Friedman, G. M., Amrel, A. J., Braun, M. and Miller, D. S., 1973. Generation of carbonate particles and laminates in algal mats: example from sea-marginal hypersaline pool, Gulf of Aqaba: *Am. Assoc. Petrol. Geol. Bull.*, v. 57, p. 541-557.

Fuller, J. G. C. M. and Porter, J. W., 1969. Evaporites and carbonates: two Devonian basins of western Canada: *Canadian Petrol. Geol. Bull.*, v. 17, p. 182-193.

Gavish, E., 1974. Geochemistry and mineralogy of a recent sabkha along the coast of Sinai, Gulf of Suez: *Sedimentology*, v. 21, p. 397-414.

- Goto, M., 1967. Oriented growth of gypsum in the Marion Lake gypsum deposit, South Australia: *J. Fac. Sci., Hokkaido Univ.*, ser. IV, Geol. Min., v. 14, p. 85-89.
- Grimm, W. D., 1962a. Ausfällung von Kieselsäure in Salinar beeinflussten sedimenten: *Zeit. Deutsch. Geol. Gesell.*, v. 118, p. 590-619.
- , 1962b. Idiomorphe Quarze als Leitminerale für Salinare Fazies: *Erdöl und Kohle*, v. 15, p. 880-887.
- Hardie, L. A. and Eugster, H. P., 1971. The depositional environment of marine evaporite: a case for shallow clastic accumulation: *Sedimentology*, v. 16, p. 187-220.
- Heimann, K. O. and Mascle, G., 1974. Les séquences de la série évaporitique messinienne: *Compt. Rend. Acad. Sci. Paris*, v. 279, ser. D., p. 1987-1990.
- Holser, W. T., 1966. Diagenetic polyhalite in recent salt from Baja California: *Am. Mineralogist*, v. 51, p. 99-109.
- Horodyski, R. J. and Vonder Haar, S. P., 1975. Recent calcareous stromatolites from Laguna Mormona (Baja California), Mexico: *J. Sediment. Petrol.*, v. 45, p. 894-906.
- Horodyski, R. J., Bloeser, B., and Vonder Haar, S., in press. Laminated algal mats from a coastal lagoon, Laguna Mormona, Baja California, Mexico: applications to the interpretation of preserved Proterozoic cyanophyte mats: *J. Sediment. Petrol.*
- Irwin, M. L., 1965. General theory of epeiric clear water sedimentation: *Am. Assoc. Petrol. Geol. Bull.*, v. 49, p. 445-459.
- James, N. P., 1972. Holocene and Pleistocene calcareous crust (caliche) profiles: criteria for subaerial exposure: *J. Sediment. Petrol.*, v. 42, p. 817-836.
- Jipa, D. C., 1974. Graded bedding in Recent Black Sea turbidites: a textural approach. *In* Degens, E. T. and Ross, D. A. (Eds.), *The Black Sea—geology, chemistry and biology*: *Am. Assoc. Petrol. Geol. Mem.* 20, p. 317-331.
- Kennett, J. P. and Watkins, N. D., 1974. Late Miocene-early Pliocene paleomagnetic stratigraphy, paleoclimatology, and biostratigraphy in New Zealand: *Geol. Soc. Am. Bull.*, v. 85, p. 1385-1398.
- Kinsman, D. J. J., 1966. Gypsum and anhydrite of Recent age, Trucial Coast, Persian Gulf. *In* Rau, J. L. (Ed.), *Second Symp. on Salt*: *Northern Ohio Geol. Soc.*, p. 302-326.
- , 1969. Modes of formation, sedimentary associations and diagnostic features of shallow-water and supratidal evaporites: *Am. Assoc. Petrol. Geol. Bull.*, v. 53, p. 830-840.
- Maiklem, W. R., Bebout, D. G., and Glaister, R. P., 1969. Classification of anhydrite—a practical approach: *Canadian Petrol. Geol. Bull.*, v. 17, p. 194-233.
- Masson, P. H., 1955. An occurrence of gypsum in southwest Texas: *J. Sediment. Petrol.*, v. 25, p. 72-77.
- Müller, G. and Stoffers, P., 1974. Mineralogy and petrology of Black Sea Basin sediments. *In* Degens, E. T. and Ross, D. A. (Eds.), *The Black Sea—geology, chemistry and biology*: *Am. Assoc. Petrol. Geol. Mem.* 20, p. 200-248.
- Neev, D. and Emery, K. O., 1967. The Dead Sea—depositional processes and environments of evaporites: *Israel Geol. Surv. Bull.*, v. 41.
- Nesteroff, W. D., 1973a. Mineralogy, petrography, distribution, and origin of the Messinian Mediterranean evaporite. *In* Ryan, W. B. F., Hsü, K. J., et al., *Initial Reports of the Deep Sea Drilling Project, Volume 13*. Washington (U. S. Government Printing Office), p. 673-694.
- , 1973b. Petrographie des evaporites Messiniennes de la Méditerranée. Comparaison des forages Joides-DSDP et des dépôts du bassin de Sicile. *In* Drooger, C. W. (Ed.), *Messinian Events in the Mediterranean: Geodynamics Sci. Rept. No. 7*, p. 111-123.
- Ogniben, L., 1954. La "Regola di Mottura" di orientazione del gesso: *Periodico Mineral.*, Anno 23, p. 53-72.
- , 1955. Inverse graded bedding in primary gypsum of chemical deposition: *J. Sediment. Petrol.*, v. 25, p. 273-281.
- , 1957. Petrografia della serie Solifera Siciliana e considerazioni geologiche relative: *Mem. Descr. Carta Geol. Italia*, v. 33.
- , 1963. Sedimenti halitico-calcitici a struttura grumosa nel Calcare di base Messiniano in Sicilia: *Giorn. Geol.*, *Ann. Mus. Geol. Bologna*, v. 31, p. 509-542.
- Orti Cabo, F. and Shearman, D. J., in press. Upper Miocene gypsum: San Miguel des Salinas, S. E. Spain: *Quaderni della Ricerea Scientifi.*
- Parea, G. C. and Ricci Lucchi, F., 1972. Resedimented evaporites in the Periadriatic Trough (Upper Miocene; Italy): *Israel J. Earth Sci.*, v. 21, p. 125-141.
- Parry, W. T., Reeves, C. C., Jr., and Leach, J. W., 1970. Oxygen and carbon isotopic composition of West Texas lake carbonates: *Geochim. Cosmochim. Acta*, v. 34, p. 824-830.
- Perthuisot, J. P., 1971. Recent polyhalite from Sebkh el Melah (Tunisia): *Nature, Phys. Sci.*, v. 232, p. 186-187.
- , 1974. Les dépôts salins de la Sebkh el Melah de Zarsis—conditions and modalités de la sédimentation évaporitique: *Rev. Géogr. Phys. Géol. Dynamique*, v. 16, p. 177-188.
- , 1975. La Sebkh el Melah de Zarsiz (Tunisie): *Travaux du Laboratoire de Géologie*, no. 9, Ecole Normale Supérieure, Paris.
- Phleger, F. B., 1969. A modern evaporite deposit in Mexico: *Am. Assoc. Petrol. Geol. Bull.*, v. 53, p. 824-829.
- Por, F. D., 1972. Hydrobiological notes on the high-salinity waters of the Sinai Peninsula: *Marine Biol.*, v. 14, p. 111-119.
- Reineck, H.-E. and Singh, I. B., 1975. *Depositional sedimentary environments*: New York (Springer-Verlag), 439 pp.
- Ricci Lucchi, F., 1973. Resedimented evaporites: indicators of slope instability and deep-basin conditions in Periadriatic Messinian (Apennines Foredeep, Italy). *In* Drooger, C. W. (Ed.), *Messinian Events in the Mediterranean: Geodynamics Sci. Rept. No. 7*, p. 142-149.
- Richter-Bernburg, G., 1973. Facies and paleogeography of the Messinian evaporites in Sicily. *In* Drooger, C. W. (Ed.), *Messinian Events in the Mediterranean: Geodynamics Sci. Rept. No. 7*, p. 124-141.
- Rochy, J.-M., 1976. Mise en évidence de nannoplancton calcaire dans certains types de gypse finement lité (balatino) du Miocene terminal de Sicile et conséquences sur la genèse des évaporites méditerranéennes de cet âge: *Compt. Rend. Acad. Sci. Paris*, v. 282, ser. D., p. 13-16.
- Ross, D. A. and Degens, E. T., 1974. Recent sediments of the Black Sea, *in* Degens, E. T. and Ross, D. A. (Eds.) *The Black Sea—geology, chemistry and biology*: *Am. Assoc. Petrol. Geol. Mem.* 20, p. 183-199.
- Ross, D. A., Neprochnov, et al., in press. *Initial Reports of the Deep Sea Drilling Project, Volume 42B*: Washington (U.S. Government Printing Office).
- Ruggieri, G., 1967. The Miocene and later evolution of the Mediterranean Sea. *In* Adams and Ager (Eds.), *Aspects of Tethyan Biogeography: Syst. Asst. Publ.* v. 7, p. 238.
- Ryan, W. B., Hsü, K. J., et al., 1973, *Initial Reports of the Deep Sea Drilling Project, Volume 13*; Washington (U.S. Government Printing Office).

- Schaller, W. T. and Henderson, E. P., 1932, Mineralogy of drill cores from the potash field of New Mexico and Texas: U.S. Geol. Surv. Bull. 833.
- Scholle, P. A. and Kinsman, D. J. J., 1974. Aragonitic and high-Mg calcite from the Persian Gulf - a modern analog Sicily as determined from analysis of intercalated carbonates: *Sedimentology*, v. 23, p. 729-760.
- Schreiber, B. C., 1974. Upper Miocene (Messinian) evaporite deposits of the Mediterranean basin and their depositional environments: Ph.D. Thesis, Rensselaer Polytechnic Institute.
- Schreiber, B. C. and Friedman, G. M., 1976. Depositional environments of upper Miocene (Messinian) evaporites of Miocene (Messinian) evaporite deposits of the Sicilian Basin: *Sedimentology*, v. 23, p. 729-760.
- Schreiber, B. C. and Kinsman, D. J. J., 1975, New observations on the Pleistocene evaporites of Montallegro, Sicily and a modern analog: *J. Sediment. Petrol.*, v. 45, p. 469-479.
- Schreiber, B. C., Catalano, R., and Schreiber, E., in press. An evaporitic lithofacies continuum: evaporitic facies observed in the upper Miocene (Messinian) deposits of the Salemi Basin (Sicily) and a modern analog: *Am. Assoc. Petrol. Geol. Mem.*, "Reefs and Evaporites."
- Schreiber, B. C., Friedman, G. M., Decima, A., and Schreiber, E., in press. The depositional environments of the upper Miocene (Messinian) evaporite deposits of the Sicilian Basin: *Sedimentology*, v. 44, p. 904-916.
- Selli, R., 1973. An outline of the Italian Messinian. *In* Drooger, C. W. (Ed.), *Messinian Events in the Mediterranean: Geodynamics Sci. Rept. No. 7*, p. 150-171.
- Shaw, A. B., 1964. *Time in stratigraphy*: New York (McGraw-Hill, Inc.).
- Shearman, D. J., 1970. Recent halite rock, Baja California, Mexico: *Inst. Mining Met., Trans.* v. 76, p. 155-162.
- , 1971. Marine evaporites: the calcium sulphate facies: Syllabus, Alberta Soc. Petrol. Geol. Seminar, Calgary, 3-5 March, 1971.
- Shearman, D. J. and Fuller, J. G., 1969. Anhydrite diagenesis, calcitization and organic laminites, Winnipegosis Formation, Middle Devonian, Saskatchewan: *Canadian Petrol. Geol. Bull.*, v. 17, p. 496-525.
- Siedlecks, A., 1972. Length slow chalcedony and relicts of sulphates—evidences of evaporitic environments in the Upper Carboniferous and Permian Beds of Bear Island, Svalbard: *Jr. Sediment. Petrol.*, v. 42, p. 812-816.
- Stewart, F. H., 1951. The petrology of the evaporites of the Eskdale no. 2 boring, east Yorkshire, Pt. III, The upper evaporite bed: *Mineral. Mag.*, v. 29, p. 557-572.
- Stoffers, P. and Kuehn, R., 1974. Red Sea evaporites: a petrographic and geochemical study. *In* Whitmarsh, R. B., Weser, O. E., Ross D. A., et al., *Initial Reports of the Deep Sea Drilling Project, Volume 23*: Washington (U.S. Government Printing Office), p. 821-847.
- Tarr, W. A., 1929. Doubly terminated quartz crystals occurring in gypsum: *Am. Mineralogist*, v. 14, p. 19-25.
- Thompson, R. W., 1968. Tidal flat sedimentation on the Colorado River delta, northwestern Gulf of California: *Geol. Soc. Am. Mem.* 107.
- Vonder Haar, S. P., 1976. Evaporites and algal mats at Laguna Mormona, Pacific Coast, Baja California, Mexico: Ph.D. Thesis, Univ. of Southern California.
- Vai, G. B. and Ricci Lucchi, F., in press. Algal crusts autochthonous and clastic gypsum in a "cannibalistic" evaporite basin: a case history from the Messinian of northern Apennines: *Sedimentology*, v. 24.
- Vonder Haar, S., in press. Gypsum in sediments. *In* Fairbridge, R. W. (Ed.), *Encyclopedia of sedimentology*: New York (Reinhold Publishing Co.).
- Vonder Haar, S. and Gorsline, D., in press. Sediments and processes in coastal ponds, Baja California: *Russel Memorial Volume on Coastal Research*, Louisiana State Univ., Baton Rouge, La.
- Walls, R. A., Harris, W. B., and Nunan, W. E., 1975. Calcareous crust (caliche) profiles and early subaerial exposure of Carboniferous carbonates, northeastern Kentucky: *Sedimentology*, v. 22, p. 417-440.
- Wardlaw, N. C. and Christie, D. L., 1975. Sulphate of submarine origin in Pennsylvanian Otto Fiord Formation of Canadian Arctic: *Canadian Petrol. Geol. Bull.*, v. 23, p. 149-171.
- West, I. M., 1964. Evaporite diagenesis in the Lower Purbeck Beds of Dorset: *Yorkshire Geol. Soc. Proc.*, v. 34, p. 315-326.